2013

Beam asymmetry Sigma for pi(+) and pi(0) photoproduction on the proton for photon energies from 1.102 to 1.862 GeV

M. Dugger

B. G. Ritchie

P. Collins

K. A. Griffioen
William and Mary, griff@physics.wm.edu

Recommended Citation

Dugger, M., Ritchie, B. G., Collins, P., Pasyuk, E., Briscoe, W. J., Strakovsky, I. I., ... & Aghasyan, M. (2013). Beam asymmetry Σ for π+ and π 0 photoproduction on the proton for photon energies from 1.102 to 1.862 GeV. Physical Review C, 88(6), 065203.

Beam asymmetry Σ for π^+ and π^0 photoproduction on the proton for photon energies from 1.102 to 1.862 GeV

M. Dugger,[2] B. G. Ritchie,[2] P. Collins,[2,*] E. Pasyuk,[2,†] W. J. Briscoe,[14] I. I. Strakovsky,[14] R. L. Workman,[14] Y. Azimov,[29] K. P. Adhikari,[28] D. Adikaram,[28] M. Aghasyan,[17] M. J. Amaryan,[28] M. D. Anderson,[37] S. Anefalos Pereira,[17] H. Avakian,[35] J. Ball,[6] N. A. Baltzell,[1,34] M. Battaglieri,[18] V. Batourine,[23,35] I. Bedlinskiy,[21] A. S. Biselli,[4,10] S. Boiarinov,[35] V. D. Burkert,[35] D. S. Carman,[35] A. Celentano,[18] S. Chandavar,[27] P. L. Cole,[15] M. Contalbrigo,[16] O. Cortes,[15] V. Crede,[12] A. D'Angelo,[19,32] N. Dashyan,[40] R. De Vita,[18] E. De Sanctis,[17] A. Deur,[35] C. Djalali,[34] D. Doughty,[7,35] R. Dupre,[20] H. Egiyan,[25,35] A. El Alaoui,[1] L. El Fassi,[1] L. Elouadrhiri,[35] P. Eugenio,[12] G. Fedotov,[33,34] S. Fegan,[18] J. A. Fleming,[9] N. Gevorgyan,[40] G. P. Gilfoyle,[31] K. L. Giovanetti,[22] F. X. Girod,[6,35] J. T. Goetz,[27] W. Gohn,[8] E. Golovatch,[33] R. W. Gothe,[34] K. A. Griffioen,[39] M. Guidal,[20] N. Guler,[28,‡] L. Guo,[11,35] K. Hafidi,[1] H. Hakobyan,[36,40] C. Hanretty,[38] N. Harrison,[8] D. Heddle,[7,35] K. Hicks,[27] D. Ho,[4] M. Holtrop,[25] Y. Ilieva,[14,34] D. G. Ireland,[37] B. S. Ishkhanov,[33] E. L. Isupov,[33] H. S. Jo,[20] K. Joo,[8] D. Keller,[38] M. Khandaker,[26] A. Kim,[23] W. Kim,[23] A. Klein,[28] F. J. Klein,[5] S. Koirala,[28] A. Kubarovsky,[8,33] V. Kubarovsky,[30,35] S. V. Kuleshov,[21,36] S. Lewis,[37] K. Livingston,[37] H. Y. Lu,[34] I. J. D. MacGregor,[37] D. Martinez,[15] M. Mayer,[28] B. McKinnon,[37] T. Mineeva,[8] M. Mirazita,[17] V. Mokeev,[33,35,§] R. A. Montgomery,[37] H. Moutarde,[6] E. Munevar,[35] C. Munoz Camacho,[20] P. Nadel-Turonski,[14,35] C. S. Nepali,[28] S. Niccolai,[20] G. Niculescu,[22] I. Niculescu,[22] M. Osipenko,[18] A. I. Ostrovidov,[12] L. L. Pappalardo,[16] R. Paremuzyan,[40,¶] K. Park,[23,35] S. Park,[12] P. Peng,[38] E. Phelps,[34] J. J. Phillips,[37] S. Pisano,[17] O. Pogorelko,[21] S. Pozdniakov,[21] J. W. Price,[3] S. Procureur,[6] Y. Prok,[28,35,38] D. Protopopescu,[37] B. A. Raue,[11,35] D. Rimal,[11] M. Ripani,[18] A. Rizzo,[19,‖] G. Rosner,[37] P. Rossi,[17,35] F. Sabatié,[6] M. S. Saini,[12] C. Salgado,[26] D. Schott,[14] R. A. Schumacher,[4] E. Seder,[8] I. Senderovich,[2] H. Seraydaryan,[28] Y. G. Sharabian,[35] G. D. Smith,[37] D. I. Sober,[5] D. Sokhan,[37] S. S. Stepanyan,[23] P. Stoler,[30] S. Strauch,[14,34] M. Taiuti,[13,**] W. Tang,[27] Ye Tian,[34] S. Tkachenko,[28,38] B. Torayev,[28] M. Ungaro,[8,35] H. Voskanyan,[40] E. Voutier,[24] N. K. Walford,[5] D. P. Watts,[9] D. P. Weygand,[35] N. Zachariou,[34] L. Zana,[25] J. Zhang,[28,35] Z. W. Zhao,[38] and I. Zonta[19,‖]

(CLAS Collaboration)

[1]*Argonne National Laboratory, Argonne, Illinois 60439, USA*
[2]*Arizona State University, Tempe, Arizona 85287-1504, USA*
[3]*California State University, Dominguez Hills, Carson, California 90747, USA*
[4]*Carnegie Mellon University, Pittsburgh, Pennsylvania 15213, USA*
[5]*Catholic University of America, Washington, DC 20064, USA*
[6]*CEA, Centre de Saclay, Irfu/Service de Physique Nucléaire, 91191 Gif-sur-Yvette, France*
[7]*Christopher Newport University, Newport News, Virginia 23606, USA*
[8]*University of Connecticut, Storrs, Connecticut 06269, USA*
[9]*Edinburgh University, Edinburgh EH9 3JZ, United Kingdom*
[10]*Fairfield University, Fairfield, Connecticut 06824, USA*
[11]*Florida International University, Miami, Florida 33199, USA*
[12]*Florida State University, Tallahassee, Florida 32306, USA*
[13]*Università di Genova, 16146 Genova, Italy*
[14]*The George Washington University, Washington, DC 20052, USA*
[15]*Idaho State University, Pocatello, Idaho 83209, USA*
[16]*INFN, Sezione di Ferrara, 44100 Ferrara, Italy*
[17]*INFN, Laboratori Nazionali di Frascati, 00044 Frascati, Italy*
[18]*INFN, Sezione di Genova, 16146 Genova, Italy*
[19]*INFN, Sezione di Roma Tor Vergata, 00133 Rome, Italy*
[20]*Institut de Physique Nucléaire ORSAY, Orsay, France*
[21]*Institute of Theoretical and Experimental Physics, Moscow 117259, Russia*
[22]*James Madison University, Harrisonburg, Virginia 22807, USA*
[23]*Kyungpook National University, Daegu 702-701, Republic of Korea*
[24]*LPSC, Universite Joseph Fourier, CNRS/IN2P3, INPG, Grenoble, France*
[25]*University of New Hampshire, Durham, New Hampshire 03824-3568, USA*
[26]*Norfolk State University, Norfolk, Virginia 23504, USA*
[27]*Ohio University, Athens, Ohio 45701, USA*
[28]*Old Dominion University, Norfolk, Virginia 23529, USA*
[29]*Petersburg Nuclear Physics Institute, 188300 Gatchina, Russia*
[30]*Rensselaer Polytechnic Institute, Troy, New York 12180-3590, USA*
[31]*University of Richmond, Richmond, Virginia 23173, USA*
[32]*Universitá di Roma Tor Vergata, 00133 Rome, Italy*
[33]*Skobeltsyn Nuclear Physics Institute, 119899 Moscow, Russia*
[34]*University of South Carolina, Columbia, South Carolina 29208, USA*

[35]*Thomas Jefferson National Accelerator Facility, Newport News, Virginia 23606, USA*
[36]*Universidad Técnica Federico Santa María, Casilla 110-V Valparaíso, Chile*
[37]*University of Glasgow, Glasgow G12 8QQ, United Kingdom*
[38]*University of Virginia, Charlottesville, Virginia 22901, USA*
[39]*College of William and Mary, Williamsburg, Virginia 23187-8795, USA*
[40]*Yerevan Physics Institute, 375036 Yerevan, Armenia*

(Received 16 August 2013; revised manuscript received 25 October 2013; published 18 December 2013; corrected 30 January 2014)

Beam asymmetries for the reactions $\gamma p \to p\pi^0$ and $\gamma p \to n\pi^+$ have been measured with the CEBAF Large Acceptance Spectrometer (CLAS) and a tagged, linearly polarized photon beam with energies from 1.102–1.862 GeV. A Fourier moment technique for extracting beam asymmetries from experimental data is described. The results reported here possess greater precision and finer energy resolution than previous measurements. Our data for both pion reactions appear to favor the SAID and Bonn-Gatchina scattering analyses over the older Mainz MAID predictions. After incorporating the present set of beam asymmetries into the world database, exploratory fits made with the SAID analysis indicate that the largest changes from previous fits are for properties of the $\Delta(1700)3/2^-$ and $\Delta(1905)5/2^+$ states.

DOI: 10.1103/PhysRevC.88.065203 PACS number(s): 13.60.Le, 14.20.Gk, 13.30.Eg, 11.80.Et

I. INTRODUCTION

Quantum chromodynamics (QCD) provides a successful description of the phenomena associated with elementary particles at high energies. Yet, extending that understanding to the low-energy, nonperturbative regime is hampered by severe limitations in our knowledge of the excitations of the nucleon and light mesons. Since the excitation spectra for nucleons and mesons still possess major gaps and ambiguities, any QCD-based description of those hadrons—and, therefore, any attempt to embed that understanding in nuclear matter—faces severe handicaps. With such deficiencies in our knowledge of nucleon and meson properties, the transition between the nonperturbative and perturbative energy regimes also remains mysterious.

This work utilizes polarized tagged photon beams in Hall B at Jefferson Lab to reveal new details of light hadron structure and to help isolate the quark and gluon angular momentum and spin contributions within hadrons. The work provides data on polarization observables in meson photoproduction. These data are absolutely necessary for progress in understanding the structure of the nucleon.

The properties of the resonances for the nonstrange baryons have been determined almost entirely from the results of pion-nucleon scattering analyses [1]. Other reactions have mainly served to fix branching ratios and photocouplings. With the refinement of multichannel fits and the availability of high-precision photoproduction data for both single- and double-meson production, identifications of some new states have emerged mainly due to evidence from reactions not involving single-pion-nucleon initial or final states [1]. However, beyond elastic pion-nucleon scattering, single-pion photoproduction remains the most studied source of resonance information.

Much of the effort aimed at providing complete or nearly complete information for meson-nucleon photoproduction reactions has been directed to measuring double-polarization observables. However, often overlooked is that the data coverage for several single-polarization observables, also vital in determining the properties of the nucleon resonance spectrum, still remains incomplete. More complete data sets for those single-polarization observables can also offer important constraints on analyses of the photoproduction reaction.

In this work, using linearly polarized photons and an unpolarized target, we provide a large set of beam asymmetry Σ measurements from 1.102–1.862 GeV in laboratory photon energy, corresponding to a center-of-mass energy W range of 1.7–2.1 GeV. As will be seen, this data set greatly constrains multipole analyses above the second-resonance region in part simply due to the size of the data set provided: with these new Σ asymmetry data from the CEBAF Large Acceptance Spectrometer (CLAS) at Jefferson Lab in Hall B, the number of measurements in the world database for the processes $\gamma p \to \pi^0 p$ and $\gamma p \to \pi^+ n$ between 1100 and 1900 MeV for E_γ is more than doubled. We will show here that there are unexpectedly large deviations between these data and some of the most extensive multipole analyses covering the resonance region. We have included these Σ data in a new partial wave analysis and will compare that analysis with competing predictions in this paper.

The paper is organized in the following manner. We give a brief background of the experimental conditions for this study in Sec. II. An overview of the methods used to extract the beam asymmetry results reported here is given in Secs. III through VII, and the uncertainty estimates for the Σ data obtained are given in Sec. VIII. The resulting data are summarized and described in Sec. IX. They are then are compared to various predictions and a new analysis presented here in Sec. X, where

[*]Present address: Catholic University of America, Washington, DC 20064, USA.
[†]Present address: Thomas Jefferson National Accelerator Facility, Newport News, Virginia 23606, USA.
[‡]Present address: Los Alamos National Laboratory, Los Alamos, New Mexico 87544, USA.
[§]Present address: Skobeltsyn Nuclear Physics Institute, 119899 Moscow, Russia.
[¶]Present address: Institut de Physique Nucléaire ORSAY, Orsay, France.
[‖]Present address: Universitá di Roma Tor Vergata, 00133 Rome Italy.
[**]Present address: INFN, Sezione di Genova, 16146 Genova, Italy.

we also compare multipoles obtained with and without including the present data set. Conclusions are presented in Sec. XI.

II. RUNNING PERIOD

The beam asymmetries for the $\gamma p \to n\pi^+$ and $\gamma p \to p\pi^0$ reactions described in this paper were part of a set of experiments running at the same time with the same experimental configuration (cryogenic hydrogen target, bremsstrahlung photon tagger [2], and CLAS [3]) called the "g8b" run period. The "g8a" and "g8b" run periods were the first Jefferson Lab experiments to use the coherent bremsstahlung technique to produce polarized photons.

During the g8b running period, a bremsstrahlung photon beam with enhanced linear polarization was incident on a 40-cm-long liquid hydrogen target placed 20 cm upstream from the center of CLAS. The enhancement of linear polarization was accomplished through the coherent bremsstrahlung process by having the CEBAF electron beam, with an energy of 4.55 GeV, incident on a 50-μm-thick diamond radiator. The photon polarization plane (defined as the plane containing the electric-field vector) and the coherent edge energy of the enhanced polarization photon spectrum were controlled by adjusting the orientation of the diamond radiator using a remotely controlled goniometer. The degrees of photon beam polarization are estimated via a bremsstrahlung calculation using knowledge of the goniometer orientation and the degree of collimation [4]. Data with an unpolarized photon beam also were taken periodically using a graphite radiator (amorphous runs). For all data runs, the CLAS magnetic field was set to 50% of its maximum nominal field, with positive particles bending outward away from the axis determined by the incident photon beam. The event trigger required the coincidence of a postbremsstrahlung electron passing through the focal plane of the photon tagger and at least one charged particle detected in CLAS.

The g8b run period was divided into intervals with different coherent edge energies, nominally set to 1.3, 1.5, 1.7, 1.9, and 2.1 GeV. In addition to the differing coherent edge energies (all measured at the same electron beam energy of 4.55 GeV), the data were further grouped into runs where the polarization plane was parallel to the floor (denoted as PARA) or perpendicular to the floor (denoted as PERP) or where the beam was unpolarized (amorphous). For the entire 1.9 GeV data set, the polarization plane was flipped between PARA and PERP automatically (auto-flip). Some of the 1.7 GeV data set was taken with auto-flip while for some runs, the polarization plane of the 1.7 GeV data was manually controlled (manual). For the 1.3 and 1.5 GeV data sets, all data used were of the manual type. (The 2.1 GeV data set was not utilized in the analysis.)

III. PARTICLE IDENTIFICATION; KINEMATIC VARIABLES

For experiments using the bremsstrahlung photon beam, the CLAS target region is surrounded by a scintillator array known as the start counter, which is used to establish the vertex time for the event [5]. Particles then pass through drift chambers, which provide tracking information that yields momentum and angular information on charged particles passing through

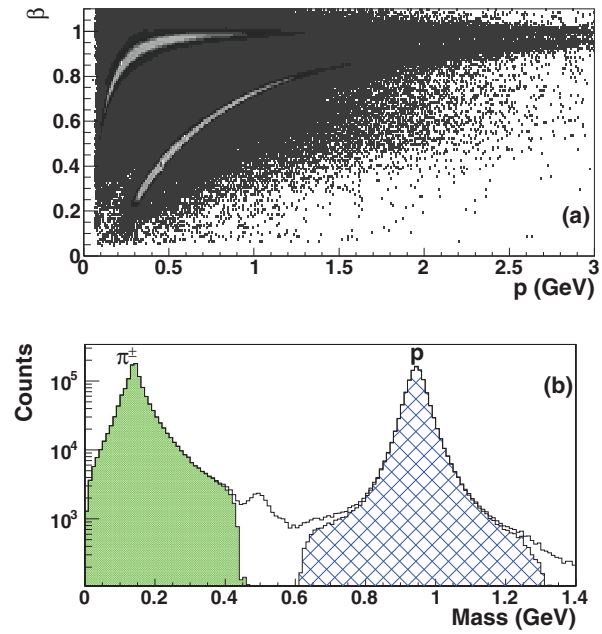

FIG. 1. (Color online) (a) Velocity β versus momentum p for all charged particles passing through CLAS in this experiment. (b) Mass of charged particles passing through CLAS in this experiment as determined by β and p, with the pions and protons identified through GPID represented by the solid shaded and crosshatched regions, respectively.

CLAS [6]. Particles then pass through the time-of-flight scintillator array [7], which, using the vertex time for the event, measures the time taken for the particle to pass from the start counter through the drift chambers. This time information determines the velocity of the charged particles passing through CLAS and, when coupled with the momentum information provided by the drift chambers, provides for determination of the mass and charge of the particle.

Using the information obtained from the start counter, drift chambers, and TOF array for each particle scattered into CLAS, particle identification was performed with the GPID algorithm (described in Ref. [8]). Plots showing β versus p and the mass distribution of the charged particles detected in CLAS, as determined by the GPID algorithm, are given in Fig. 1. As discussed in Ref. [8], the GPID method uses the CLAS-measured momentum of the particle whose identity is to be determined, and calculates theoretical values of β for the particle to be any one of all possible identities. Each one of the possible identities is tested by comparing the theoretical value of β for a given particle type (using the reconstructed momentum information from CLAS) to the measured value of β (as determined from time-of-flight information). The particle is assigned the identity that provides the closest expected value of β to the empirically measured value of β. The identification for protons and pions is illustrated in Fig. 1.

IV. MISSING MASS RECONSTRUCTION FOR π N FINAL STATES

The kinematic quantities determined from the time-of-flight and drift chamber systems yield good momentum definition for

the proton and π^+. The energy and momentum determined for each particle by CLAS were corrected for energy lost by that particle in passing through the material in both the target cell and the start counter in order to reconstruct the momentum at the vertex where the photoproduction reaction occurred using the standard CLAS algorithm for those corrections, ELOSS [9]. In addition to the energy loss correction, a CLAS momentum correction was used. The CLAS momentum correction optimized the momentum determination through kinematic fitting.

The scattering angle and momentum information for each particle was used to construct a missing mass M_X based on the assumption that the reaction observed was $\gamma p \to \pi^+ X$ or $\gamma p \to pX$, where X is the other body in the two-body final state using the relation

$$M_X = \sqrt{m_{\pi^+}^2 + m_p^2 + 2E_\gamma m_p - 2E_{\pi^+}(m_p + E_\gamma) + 2E_\gamma p_{z\pi^+}}$$

for the $\gamma p \to \pi^+ X$ reaction, and

$$M_X = \sqrt{2m_p^2 + 2E_\gamma m_p - 2E_p(m_p + E_\gamma) + 2E_\gamma p_{zp}}$$

when the reaction is $\gamma p \to pX$, where M_X is the mass of the missing particle, E_γ is the incident photon energy, m denotes mass, p is the momentum, p_z denotes the z component of the momentum, and subscripts define the particle type.

Based on these assumptions, the missing mass spectrum for data in the full spectrometer acceptance for all photon energies within the 1.3 GeV coherent edge setting is shown in Fig. 2. The neutron and π^0 peaks are clearly seen.

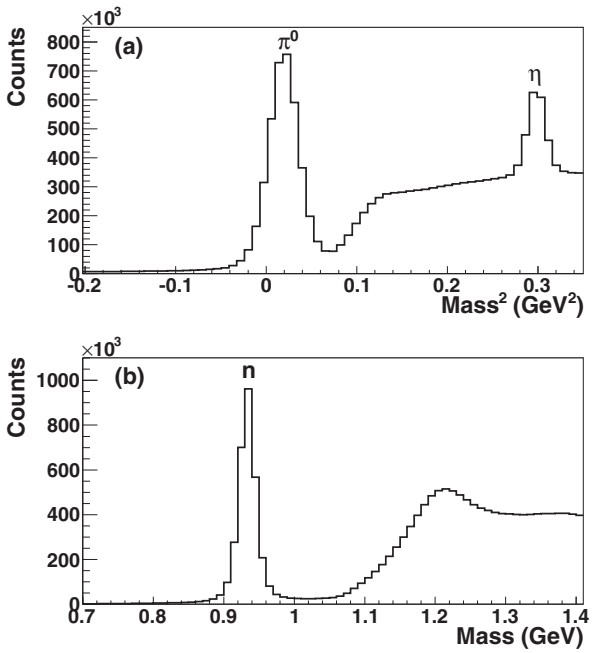

FIG. 2. (a) Spectrum of squared missing mass M_X^2 from the reaction $\gamma p \to pX$. (b) Missing mass M_X from the reaction $\gamma p \to \pi^+ X$. The π^0, η, and neutron peaks are indicated on the plots.

V. FOURIER MOMENT TECHNIQUE FOR EXTRACTING BEAM ASYMMETRY Σ

Traditionally, beam asymmetries have been extracted by breaking the azimuthal acceptance of the spectrometer into a very large number of bins, extracting the meson yields for those bins, and then fitting that distribution of yields with a linear-plus-cosine expression to determine Σ. As a more efficient procedure, the beam asymmetries for this experiment were extracted using a Fourier moment analysis of the azimuthal (φ) scattering angle distributions of the particles detected in CLAS. An overview of the technique used to extract the beam asymmetries is presented in Appendix A.

Using the moment method, the beam asymmetry is written as

$$\Sigma = \frac{\tilde{Y}_{\perp 2} - \tilde{Y}_{\parallel 2}}{\frac{P_\parallel}{2}(\tilde{Y}_{\perp 0} + \tilde{Y}_{\perp 4}) + \frac{P_\perp}{2}(\tilde{Y}_{\parallel 0} + \tilde{Y}_{\parallel 4})}, \quad (1)$$

where $\tilde{Y}_{\perp n}$ ($\tilde{Y}_{\parallel n}$) is the normalized meson yield having incident photons polarized perpendicular (parallel) to the laboratory floor, with each event weighted by $\cos(n\varphi)$, and having the degree of photon polarization given as $P_\perp$ ($P_\parallel$).

Equation (1) is the principal result for this method. With this approach, rather than partitioning the data for a given E_γ and $\cos(\theta)$ into various φ bins, all the data for a given E_γ and $\cos(\theta)$ are used simultaneously to determine the beam asymmetry Σ for the reaction of interest.

VI. YIELD DETERMINATION FOR EACH KINEMATIC BIN

To determine the π^0 yields, a technique very similar to the one used for the g1c experiment of extracted differential cross sections for π^0 photoproduction off the proton [10] was employed. The g1c experiment utilized the same CLAS detector and bremsstrahlung photon tagger as the g8b experiment, but had an 18-cm-long liquid hydrogen target placed at the center of CLAS, and only used unpolarized incident photons.

Following the previous discussion, the beam asymmetries were determined for a particular photon energy and $\cos(\theta)$ bin, which we call a kinematic bin. For each missing mass spectrum within each kinematic bin, the π^0 yield was extracted by removing the background under the peak. It was assumed that the background in the missing mass spectra arises from two particular types of events:

(i) Events arising from accidental coincidences between CLAS and the photon tagger;
(ii) Events arising from two-pion photoproduction via the reaction $\gamma p \to p\pi^+\pi^-$.

The spectrum for accidental coincidences can be determined by looking at events that fell outside the designated trigger window. From experience with the g1c experiment, the background coming from accidentals within the g8b data set was approximated as being linear in missing mass. Figure 3 shows an example of the background subtraction from the CLAS published g1c pion differential cross sections [10], where the accidental contribution was determined by looking

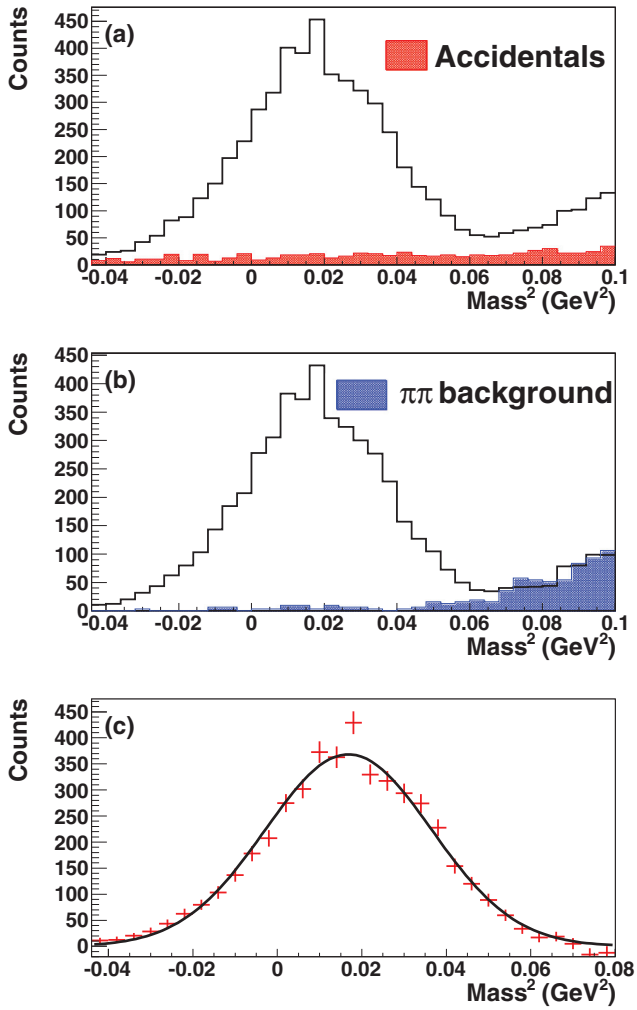

FIG. 3. (Color online) Yield extraction examples from previously published `g1c` π^0 differential cross sections [10]. Shown are data for the π^0 yield extraction for $E_\gamma = 1.425$ GeV and $\cos\theta^p_{\text{c.m.}} = -0.45$. (a) is the missing mass yield for this bin, with the accidental contribution displayed in shaded region. The accidental contribution is seen to be small and linear. (b) shows the missing mass distribution with the accidental contributions subtracted; the shaded region indicates the 2-π contribution determined. (c) shows the extracted π^0 yield after contributions for accidentals and two-pion photoproduction have been subtracted from the missing mass distribution.

at events that fell outside the designated trigger window. As can be seen in Fig. 3 the assumption that the accidentals are well modeled by a linear function is reasonable.

To determine the two-pion background, data for the reaction $\gamma p \to p\pi^+\pi^-$ were selected by requiring that each particle in the final state had to be identified through normal particle ID procedures, that the same incident photon was chosen for each particle, and that the missing mass was consistent with zero; the criterion for consistency with zero mass was if the mass m^2_Y, in the reaction $\gamma p \to p\pi^+\pi^- Y$ was less than 0.005 GeV^2 and greater than -0.01 GeV. These selected data were used to determine the *shape* of the $\pi^+\pi^-$ component of the background for the $\gamma p \to p\pi^0$ reaction in each kinematic bin.

The background subtraction for the π^0 was then performed in the following manner.

(i) The spectrum of missing mass M_X in the $\gamma p \to pX$ reaction was fitted by a functional form that included the linear approximation of the accidentals and the shape determined for the charged background noted above. A total of three parameters were varied: two parameters for the accidental contribution (modeled by a linear function) and one parameter for the *magnitude* of the charged background.

(ii) The backgrounds determined in the previous step were subtracted from the yield.

(iii) The background subtracted yield was then fit by a Gaussian and the standard deviation and centroid of the peak were determined.

(iv) The region of the histogram resulting from step (iii) that was within three times the standard deviation of the peak centroid was then determined to be the $\gamma p \to p\pi^0$ yield in the extracted π^0 peak.

For the extraction of the yield of the neutron peak from the reaction $\gamma p \to \pi^+ X$, it was found that the 2π background was negligible, and the only significant background was from accidentals. For this reason, only a linear approximation of the accidentals was included in the background determination for the neutron.

An example of the background subtraction for both neutron and π^0 extraction can be seen in Fig. 4.

VII. RELATIVE NORMALIZATION

For the measurement of beam asymmetry, knowledge of the absolute number of incident photons is not required. Instead, only the relative photon normalization between PARA and PERP running conditions is necessary. In order to obtain the relative photon normalization of PARA to PERP, a rough π^0 measurement was used, where rough π^0 is defined as any event detected from $\gamma p \to pX$ with missing mass M_X between 0.0 and 0.25 GeV and, in this instance, $0 \leqslant \cos(\theta^X_{\text{c.m.}}) \leqslant 1$, where $\cos(\theta^X_{\text{c.m.}})$ is the meson center-of-mass scattering angle.

For the determination of the relative normalization, the more conventional approach of binning the rough π^0 data into azimuthal angle bins was used. The data were binned in the same E_γ bins as for the moment extraction method, and in addition, the data were binned further into 36 azimuthal bins.

Once the yield for π^0 mesons was determined for each the running conditions, two quantities for each $\{E_\gamma, \varphi\}$ bin were formed,

$$g_\perp \equiv \frac{Y_\perp}{Y_a}$$

and

$$g_\parallel \equiv \frac{Y_\parallel}{Y_a}.$$

These were fit by

$$g_\perp = A_\perp[1 + B\cos(2\varphi)]$$

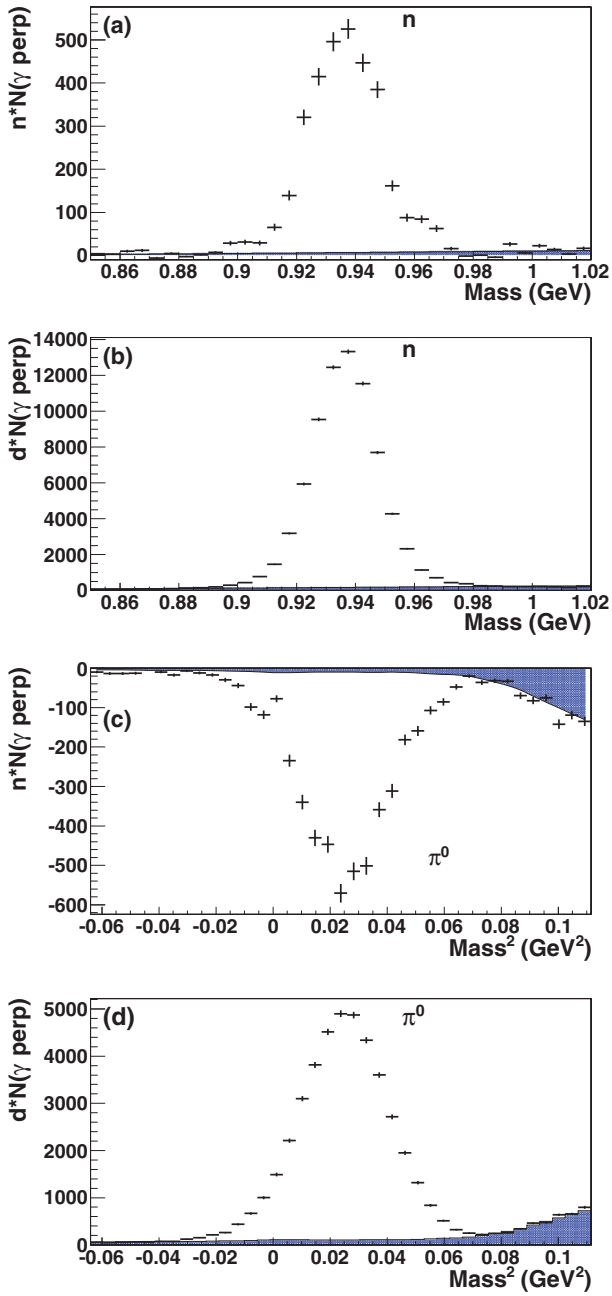

FIG. 4. (Color online) Extraction of the quantities n and d [defined in Appendix A Eq. (A20)] for neutron (top two panels) and π^0 (bottom two panels) for the kinematic bin $\theta^{\pi}_{\text{c.m.}} = 123^{\circ}$ and $E_{\gamma} = 1229$ MeV. (a) and (b) Reaction $\gamma p \to \pi^+ n$. The x axis is missing mass M_X from the reaction $\gamma p \to \pi^+ X$. (c) and (d) Reaction $\gamma p \to p\pi^0$. The x axis is squared missing mass M_X^2 from the reaction $\gamma p \to pX$. The shaded region in each plot represents contributions from background.

and

$$g_{\parallel} = A_{\parallel}[1 - B\cos(2\varphi)],$$

where $A_{\parallel} = N_{\parallel}/N_a$, $A_{\perp} = N_{\perp}/N_a$, $B = P\Sigma$, and $N_{\perp}, N_{\parallel}, N_a$ represent the number of incident photons for the PERP, PARA, and amorphous running conditions respectively.

The values of A taken from the parallel polarized beam orientation were divided by the values derived from the perpendicular orientation. The fractional values of $A_{\parallel}/A_{\perp}$ were found for each energy to determine the value of $N_{\parallel\gamma}/N_{\perp\gamma}$ from the relation $A_{\parallel}/A_{\perp} = N_{\parallel\gamma}/N_{\perp\gamma}$.

VIII. UNCERTAINTIES

The statistical uncertainties for Σ were obtained using the expressions given in Appendix A3. Systematic uncertainties for Σ are dominated by the systematics of the polarization and relative normalization since many of the experimental quantities cancel in the ratio Σ.

The relative normalization was primarily dependent upon the total number of $\gamma p \to pX$ events having a missing mass (mass X) between 0 and 0.25 GeV. The statistics for such events were quite good and we take the systematic uncertainty of the relative normalization as being negligible.

One possible systematic error could come from imperfect knowledge of the orientation of beam polarization. To study the orientation of the beam polarization we took rough π^0 measurements for each orientation of the beam polarization (PERP and PARA) and normalized each type by the rough π^0 results from the amorphous runs. Using the entire set of runs from the 1.3 GeV coherent edge setting, the resulting rough π^0 normalized yields were placed in 90 φ bins, and 50 MeV wide photon energy bins. The resulting φ distributions were then fit by the function $A[1 + B\cos(2\varphi + 2C)]$, with A, B, and C being fit parameters. From the fit we were able to extract the possible azimuthal offset by reading out parameter C. Figure 5 shows the resulting fit for both orientations at photon energy of 1275 MeV. (The figure also clearly shows

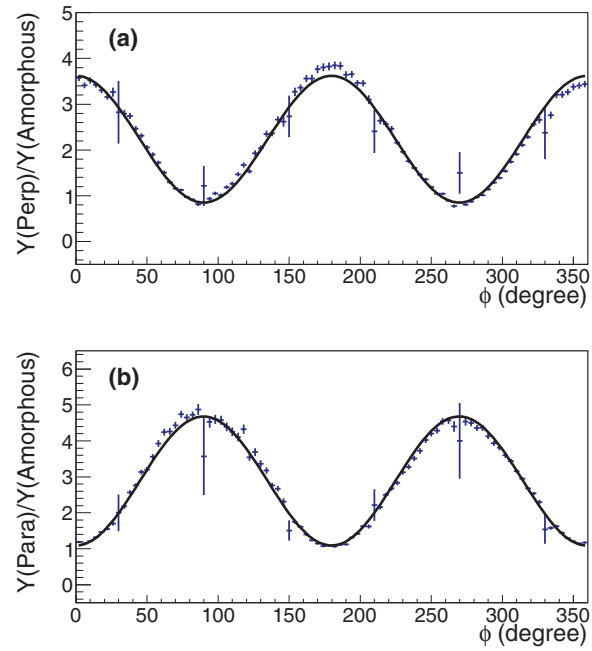

FIG. 5. (Color online) Rough π^0 normalized yields for forward center-of-mass angles. (a) shows the normalized yields for runs with the PERP polarization orientation, while (b) shows the normalized yields for runs with the PARA orientation.

the six-sector structure of CLAS.) We performed the fitting procedure for five energy bins from the 1.3 GeV data, took the weighted average, and obtained a possible systematic error in the polarization orientation of 0.07 ± 0.04 degrees. Since the possible systematic error is so small, we have assumed that such an error has a negligible effect on the beam asymmetry measurements.

The overall accuracy of the estimated photon polarization is difficult to determine. However, the consistency of the bremsstrahlung calculation could be checked by comparing predicted and measured polarization ratios for adjacent coherent edge settings in regions where overlapping energies exist. After consistency corrections were applied [11], the estimated value for the photon polarization was self-consistent to within 4%. Therefore, the estimated systematic uncertainty in the photon polarization is taken to be 4%.

To test the dependence of the Fourier moment method on the polarization values, rough π^0 beam asymmetries from the moment method were compared to the beam asymmetries obtained using the φ-bin method (averaged over polarization orientations). As in Sec. VII, a rough π^0 azimuthal distribution was extracted for each tagger energy counter (E-counter). This time, however, the rough π^0 extraction was performed for the backward center-of-mass pion-angles $[-1 \leqslant \cos(\theta^X_{\text{c.m.}}) \leqslant 0]$, as well as the forward center-of-mass pion-angles $[0 \leqslant \cos(\theta^X_{\text{c.m.}}) \leqslant 1]$.

For each case (forward and backward angle events), the polarized photon data were divided by the corresponding distribution from amorphous data. As done in Sec. VII, the ratios for the azimuthal distributions were then fit by the expression

$$A\,[1 + B\cos(2\varphi)]\,, \tag{2}$$

where A and B were parameters of the fit. The value of beam asymmetry was then determined by $\Sigma = B_\perp / P_\perp$ ($\Sigma = -B_{||}/P_{||}$).

The values of Σ determined from the φ bin for each polarization orientation were averaged to obtain an average Σ value. The average Σ value obtained from the φ-bin method is compared to the beam asymmetries determined by the moment method, as seen in Fig. 6. The top panel of Fig. 6 shows the rough π^0 beam asymmetries as a function of energy counter for the forward center-of-mass angles, and the backward center-of-mass angles are shown on the bottom panel. In each panel of Fig. 6 the black points are Σ determined by the φ-bin method and the open circles represent Σ determined from the moment method. A visual inspection of the plots given in Fig. 6 shows that the φ bin and moment methods give very similar results.

To quantify the level of agreement between the two methods, the Σ results from the moment method were divided by those of the φ-bin method on an E-counter by E-counter basis. A frequency plot of the resulting Σ fractions (Σ from moment method divided by Σ from φ-bin method) was created for forward and backward center-of-mass angles of the π^0. In the top panel of Fig. 7 the frequency of Σ fractions for forward angles is shown, while the bottom panel is the frequency plot for backward angles. A Gaussian was fit to each distribution of Fig. 7 with the results shown in Table I.

Since the beam asymmetry results from the moment method are well within 1% of the beam asymmetry results

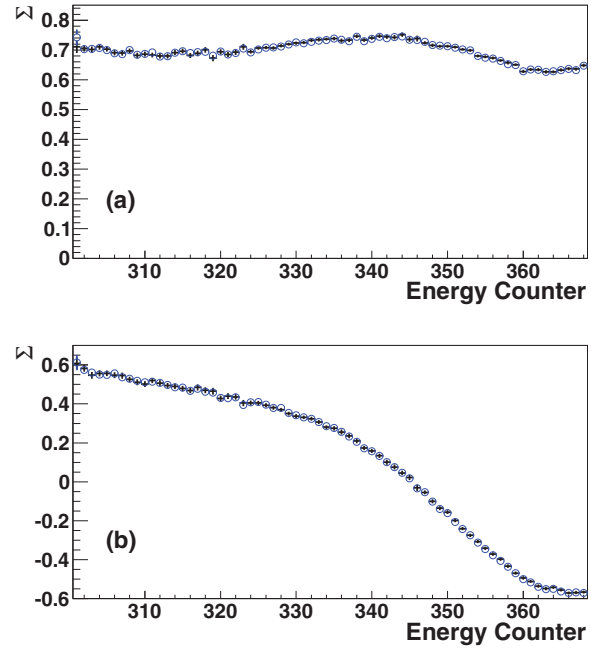

FIG. 6. (Color online) Rough π^0 beam asymmetries Σ for forward (a), and backward (b) center-of-mass angles determined for polarized photons associated with the indicated photon tagger energy counter. Blue open circles represent values of Σ determined by the Fourier moment method, while black points represent values of Σ determined by the ϕ-bin method averaged over polarization orientations.

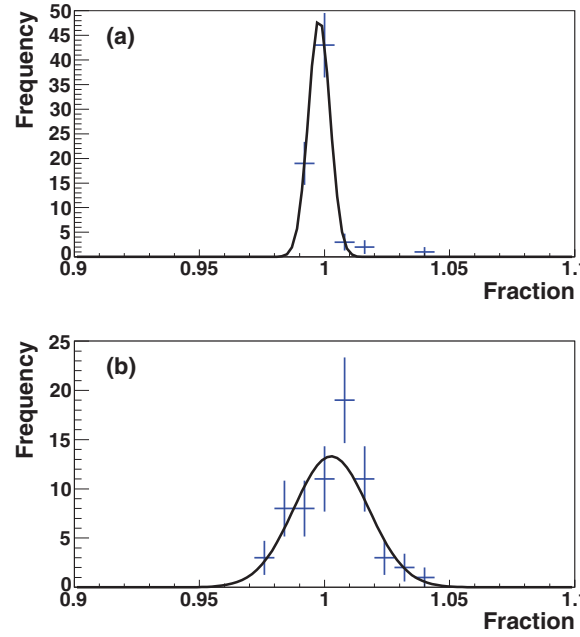

FIG. 7. (Color online) Frequency distribution for the rough π^0 data shown in Fig. 6 of the ratios of Σ from the Fourier moment method divided by Σ obtained from the ϕ-bin method for each photon tagger energy counter. (a) Forward center-of-mass angles. (b) Backward center-of-mass angles. A Gaussian fit to each of these distributions is also shown.

TABLE I. Gaussian parameters of the fit to the ratios of the results for Σ using the moment method to Σ determined by the φ-bin method on an E-counter by E-counter basis.

Center-of-mass angles	Center	σ
Forward	0.9978(3)	0.0043(4)
Backward	1.003(2)	0.015(2)

coming from the average value (parallel and perpendicular orientations) determined by the φ-bin method, we can safely say that the systematic uncertainty of the moment method due to polarization is nearly identical to the systematics one obtains when simply averaging the beam asymmetry from each polarization orientation. Thus, the fractional uncertainty of each polarization systematic uncertainty (each estimated as 4%) is added in quadrature to obtain an estimate of the systematic uncertainty in the beam asymmetry of 6%.

IX. RESULTS

The CLAS beam asymmetries obtained here for $\vec{\gamma}p \to p\pi^0$ (700 data points represented as filled circles) are compared in Figs. 8 and 9 with previous data from Bonn [12,13] (open circles), Yerevan [14–19] (open triangle), GRAAL [20] (open squares), CEA [21] (filled squares), DNPL [22,23] (crosses), and LEPS [24] (asterisks). The results for the reaction $\gamma p \to n\pi^+$ CLAS beam asymmetries (386 data points shown as filled circles) are compared in Fig. 10 to previous data from GRAAL [25] (open squares), Yerevan [26] (open triangles), CEA [21] (filled squares), and DNPL [23] (crosses). Only those world data that are within ±3 MeV of the CLAS photon energies E_γ are shown. In addition to the data, phenomenological curves are included in the above mentioned figures and will be discussed further below.

For the CLAS π^0 data obtained here, the Yerevan results agree well except for a few points at E_γ =1265, 1301, and

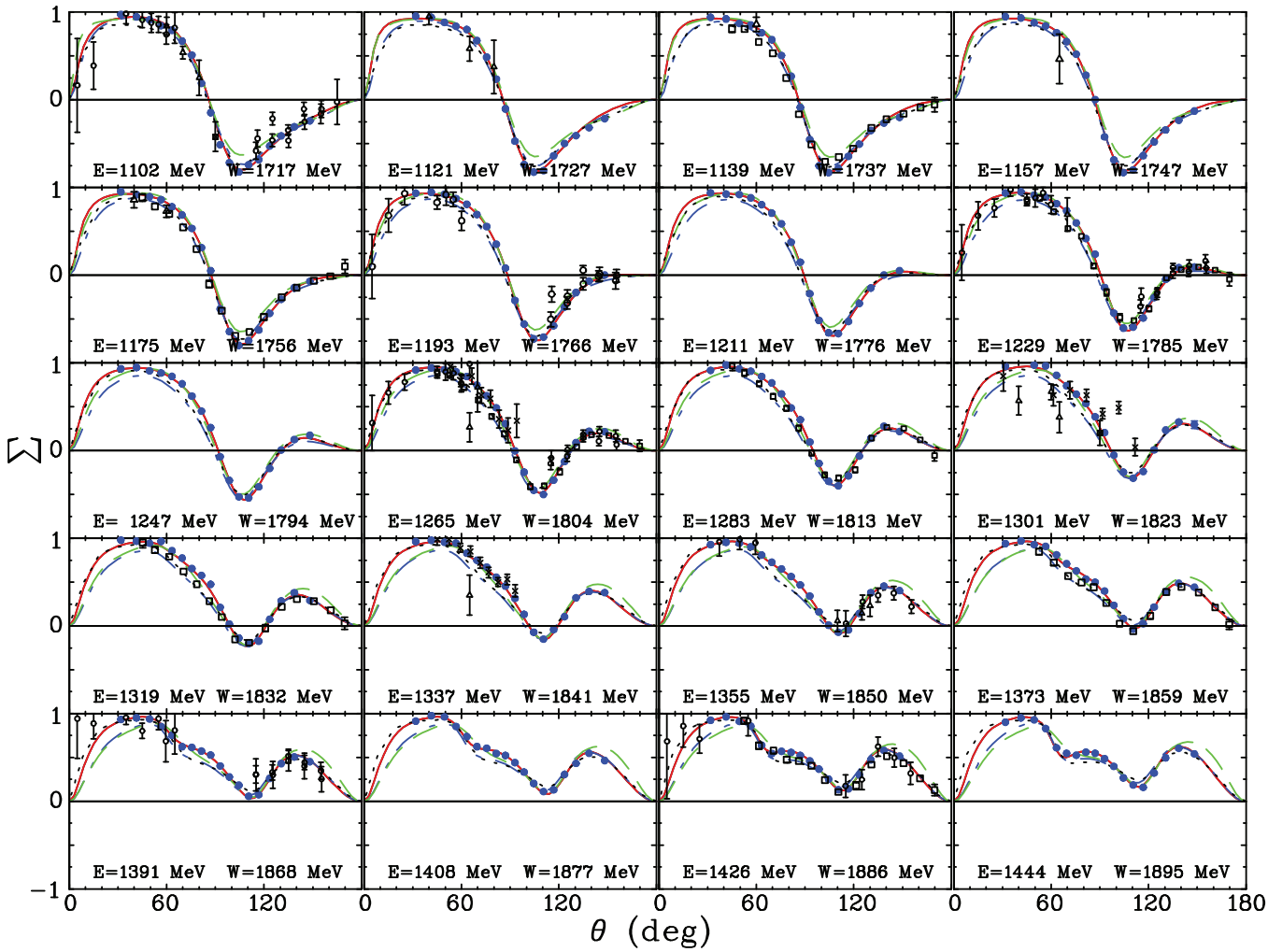

FIG. 8. (Color online) Beam asymmetry Σ for $\vec{\gamma}p \to \pi^0 p$ at E_γ = 1102–1444 MeV versus pion center-of-mass production angle. Photon energy is indicated by E, while the center-of-mass total energy is indicated by W. Red solid (blue dash-dotted) lines correspond to the SAID DU13 (CM12 [27]) solution. Green dashed (black short-dashed) lines give the MAID07 [28] (BG2011-02 BnGa [29]) predictions. Experimental data are from the current (filled circles), Bonn [12,13] (open circles), Yerevan [14–19] (open triangle), GRAAL [20] (open square), CEA [21] (filled square), DNPL [22,23] (cross), and LEPS [24] (asterisk). Plotted uncertainties are statistical. The plotted points from previously published experimental data [30] are those data points within 3 MeV of the photon energy indicated on each panel.

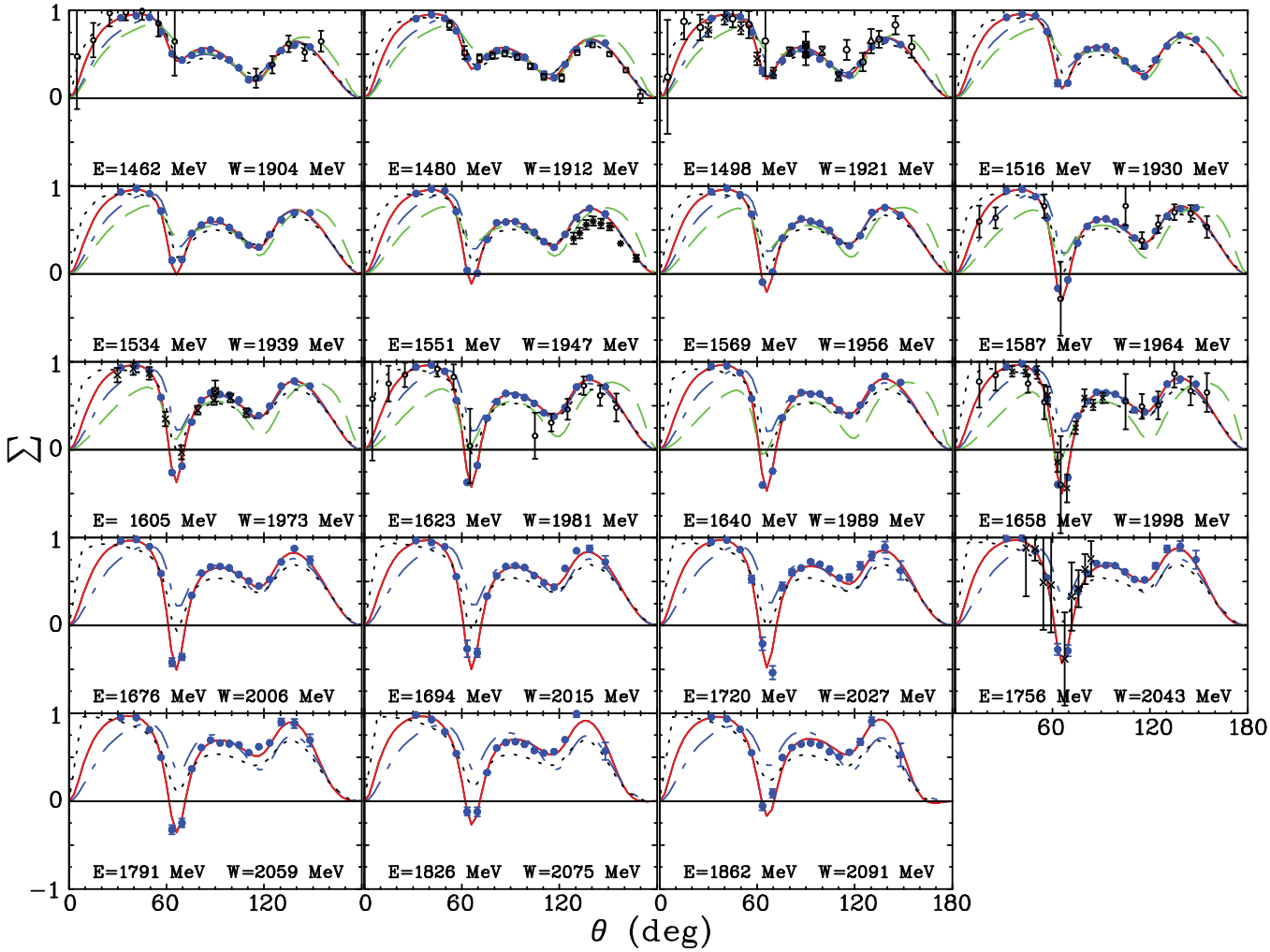

FIG. 9. (Color online) Beam asymmetry Σ for $\vec{\gamma}p \to \pi^0 p$ at $E_\gamma = 1462$–1862 MeV versus pion center-of-mass production angle. The photon energy is shown as E. Notation as in Fig. 8.

1337 MeV. The Bonn data are comprised of two separate analyses [12,13], one published in 2009 [12] and another published in 2010 [13]. The earlier analysis only used data from one coherent peak position (1305 MeV) and excluded the very forward-going pion data. The most recent analysis included data from two coherent peak positions (1305 and 1610 MeV) and included the very forward-going pion data. Typically, the CLAS results agree within error bars of the Bonn data, and where there is disagreement, it is almost always with the earlier 2009 results. The data obtained here are in very good agreement with DNPL at $E_\gamma = 1337$ MeV and tend to be within error bars for all other energies except for $E_\gamma = 1301$ MeV, where several DNPL points are systematically larger than the CLAS results. In particular, the data obtained here confirm the magnitude of the sharp structure seen in the DNPL data near 60° for photon energies greater than about $E_\gamma = 1600$ MeV. The LEPS results ($E_\gamma =$ 1551 MeV, backward angles), as well as the GRAAL results look systematically smaller when compared to CLAS.

The π^+ data obtained here tend to agree well with the previous data except for a few points. Out of the 34 points from GRAAL, easily identifiable differences between GRAAL [25] and CLAS occur for four with $E_\gamma = 1148$ MeV ($\theta = 114°$, 122°, 145°, and 150°), along with a single point at $E_\gamma = 1400$ ($\theta = 90°$). The single CEA [21] point at $E_\gamma = 1400$ MeV ($\theta = 90°$) is systematically low when compared to CLAS. For the single Yerevan measurment of beam asymmetry [26], the agreement is good. Comparisons between CLAS and DNPL [23] are mixed. The DNPL results were taken with two different sets of beam energies. There was a low-energy data set from DNPL with photon energies ranging from 520 to 1650 MeV, and a high energy data set with energies between 1650 and 2250 MeV. Because the DNPL energy ranges overlap for $E_\gamma =$ 1650 MeV, they report two sets of beam asymmetries for that energy. The DNPL data from the low-energy data set agrees well with CLAS except for a single point at $E_\gamma = 1400$ MeV ($\theta = 75°$), while the agreement between CLAS and the DNPL high-energy data set is sometimes poor. In particular, at $E_\gamma = 1649$ MeV, the DNPL points that are systematically high (low) compared to CLAS occurring at $\theta = 30°$, 40°, 75° ($\theta = 105°$, 115°) are all from the DNPL high-energy data set, while the agreement between CLAS and DNPL at

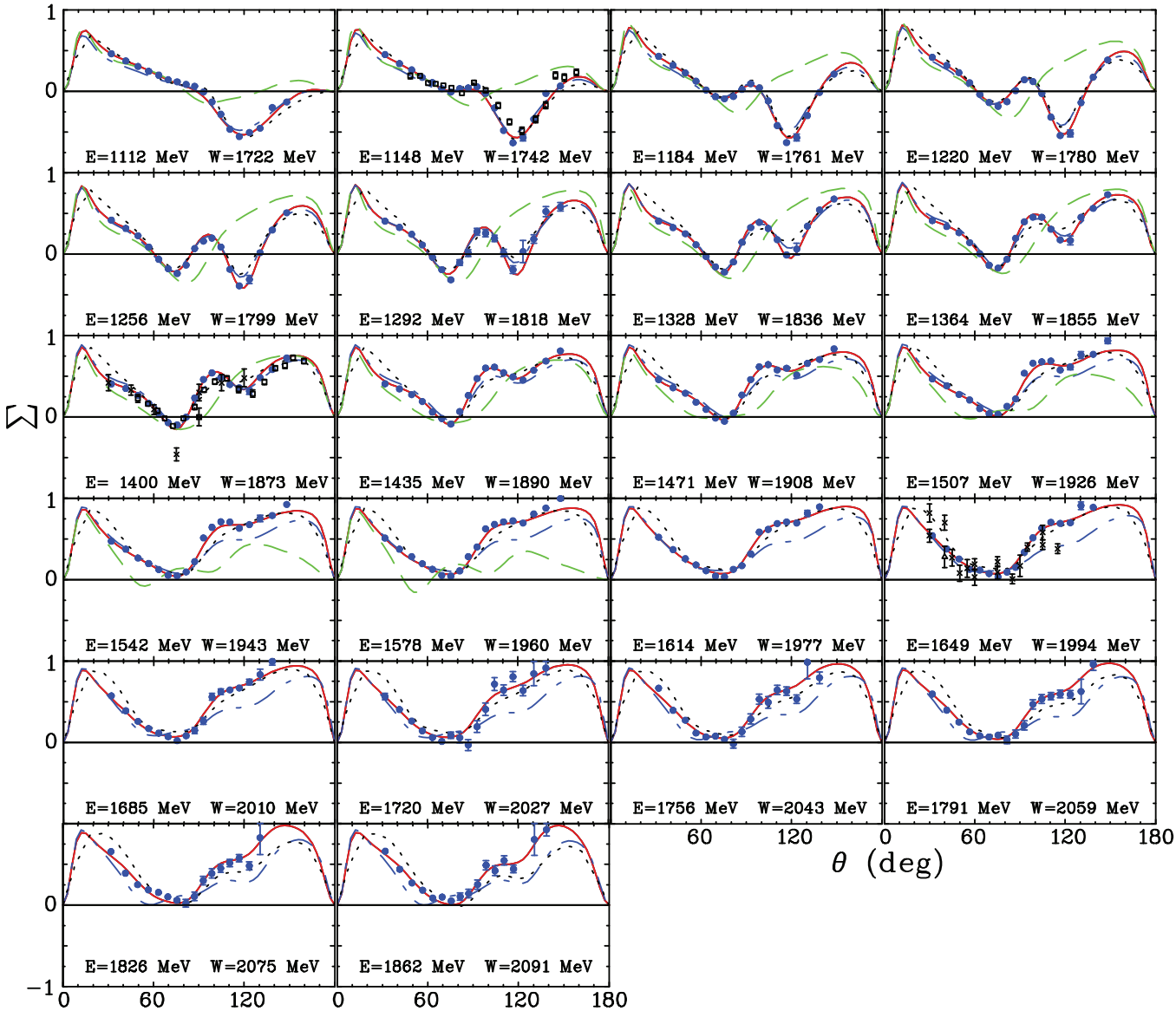

FIG. 10. (Color online) Beam asymmetry Σ for $\vec{\gamma}p \to \pi^+ n$ at $E_\gamma = 1112$–1862 MeV versus pion center-of-mass production angle. The photon energy is shown as E. Red solid (blue dash-dotted) lines correspond to the SAID DU13 (CM12 [27]) solution. Green dashed (black short-dashed) lines give the MAID07 [28] (BG2011-02 BnGa [29]) predictions. Experimental data are from the current (filled circles), GRAAL [25] (open square), Yerevan [26] (open triangle), CEA [21] (filled square), and DNPL [23] (cross). Plotted uncertainties are statistical. The plotted points from previously published experimental data [30] are those data points within 3 MeV of the photon energy indicated on each panel.

$E_\gamma = 1649$ MeV from the low-energy data set is in good agreement.

Briefly, then, the new CLAS measurements generally are in agreement with older results within uncertainties, but the results presented here are far more precise and provide finer energy resolution.

X. COMPARISON TO FITS AND PREDICTIONS

A. Comparison to phenomenological models

In Figs. 8–10, the Σ data are shown along with predictions from previous SAID [27], MAID [28] (up to its stated applicability limit at a center-of-mass energy $W = 2$ GeV, corresponding to $E_\gamma = 1.66$ GeV), and the Bonn-Gatchina (BnGa, [29]) multipole analyses. Also shown are the results of an updated SAID fit (DU13), which includes the new data reported here. In order to increase the influence of these new precise data, the CLAS data reported here were weighted by an arbitrary factor of 4 in the fit. Figures 11 and 12 show fixed angle excitation functions for $\vec{\gamma}p \to \pi^0 p$ and $\vec{\gamma}p \to \pi^+ n$.

For energies below that of the data presented in this paper, the neutral-pion production data are well represented by predictions from the multipole analyses up to a center-of-mass energy of about 1500 MeV. Above this energy, large differences are seen at very forward angles. The data appear to favor the SAID and BnGa predictions, with large differences

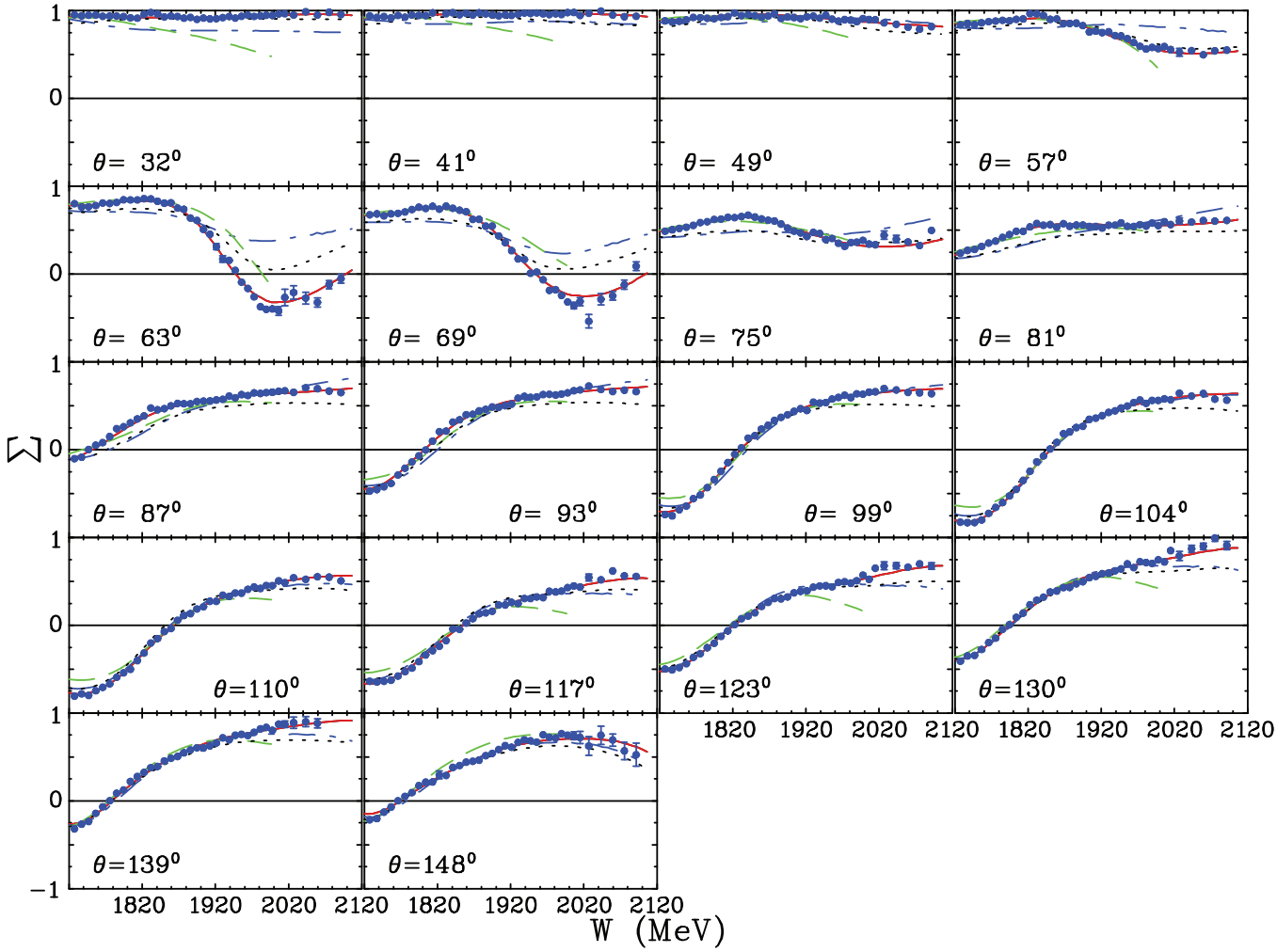

FIG. 11. (Color online) Fixed angle excitation functions of the beam asymmetry Σ for $\vec{\gamma}p \to \pi^0 p$. The pion center-of-mass production angle is shown. Notation as in Fig. 8.

between the SAID and BnGa values mainly at angles more forward than are reached in the present experiment. Pronounced dips seen in Figs. 8 and 9 for the reaction $\gamma p \to \pi^0 p$, are qualitatively predicted by the three multipole analyses. These dips develop at angles slightly above 60° and slightly below 120° (note that these angles are related by the space reflection transformation $\theta \to \pi - \theta$). Our data confirm this feature suggested by earlier measurements, however those previous data were not precise enough to establish the sharpness of the dips. The revised SAID fit (DU13) now has these sharp structures. Below we shall discuss in more detail a possible source of the dip structure seen in the data.

For the charged-pion reaction, the MAID predictions are surprisingly far from the data over most of the measured energy range, and particularly at more backward angles. Over much of this range the SAID, BnGa, and revised SAID curves are nearly overlapping.

The fit χ^2 per data point χ^2/N_p for DU13 is significantly improved over that from the CM12 SAID prediction [27]. The comparison given in Table II shows that, for the new DU13 fit, χ^2/N_p for the $\pi^0 p$ channel is 2.77 and χ^2/N_p for the $\pi^+ n$ channel is 2.77, an improvement by over an order of magnitude for that χ^2/N_p statistic when compared with the CM12 prediction. While the fit χ^2 per datum is 2.77 when solely compared to the new CLAS data reported here, Table II

TABLE II. Comparison of χ^2 per data point for the beam asymmetry Σ for the $\pi^0 p$ and $\pi^+ n$ channels using the predictions of the CM12 SAID solution [27] and the results of a fit (DU13) to the CLAS data reported here. Comparisons are provided for the CLAS data, previously published data, and for a data set containing both the CLAS data (weighted by a factor of 4) and the previously published data. The number of data points used in each comparison is indicated by N_p.

Data	Solution	$\Sigma(\pi^0 p)$ χ^2/N_p	$\Sigma(\pi^+ n)$ χ^2/N_p
New CLAS	DU13	$1940/700 = 2.77$	$1070/386 = 2.77$
data only	CM12	$53346/700 = 76.2$	$11795/386 = 30.6$
Previous	DU13	$1531/654 = 2.34$	$738/201 = 3.67$
data only	CM12	$1704/654 = 2.61$	$801/201 = 3.99$
CLAS and	DU13	$3471/1354 = 2.56$	$1808/587 = 3.08$
previous data	CM12	$55050/1354 = 40.7$	$12596/587 = 21.5$

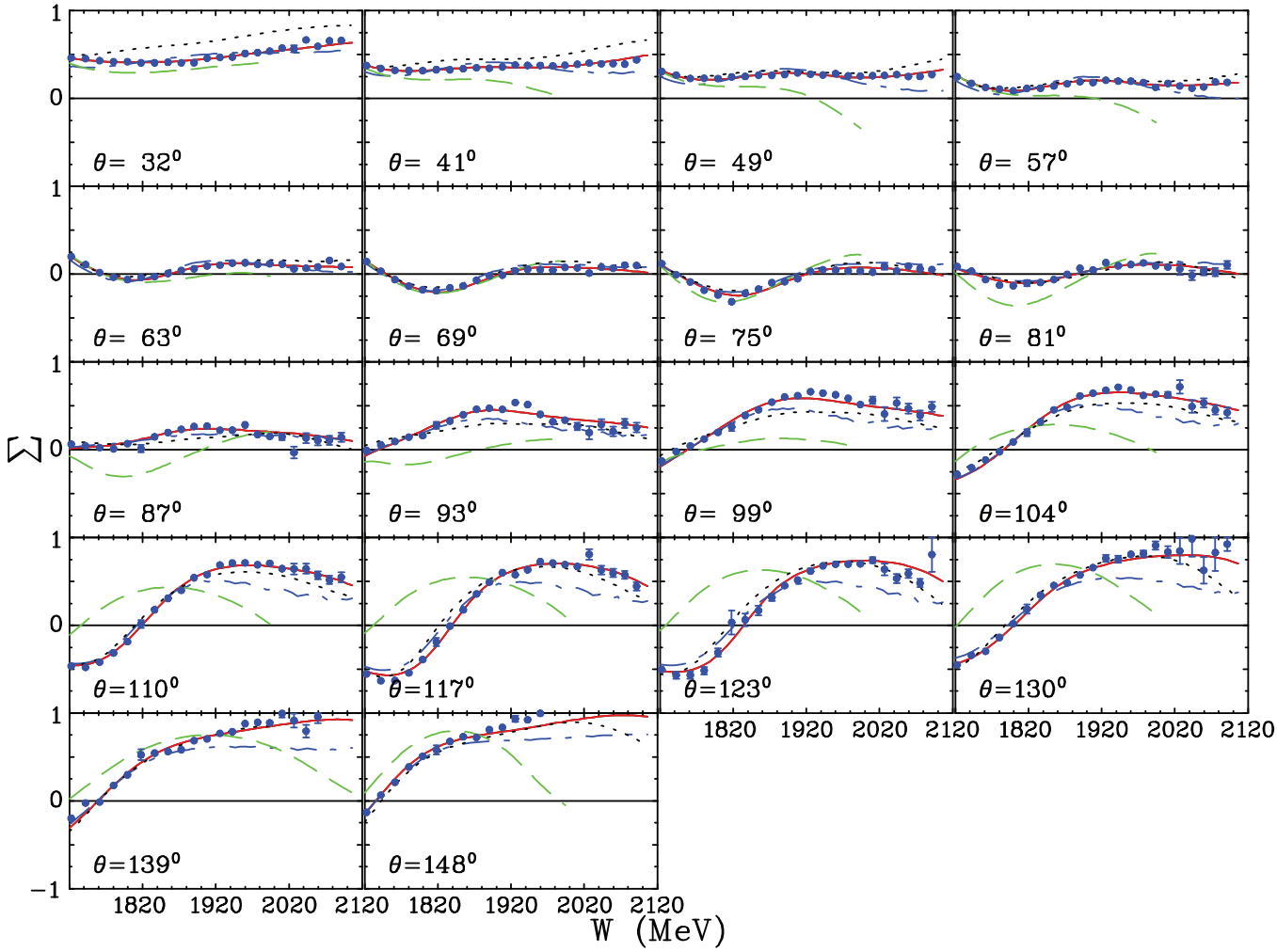

FIG. 12. (Color online) Fixed angle excitation functions of the beam asymmetry Σ for $\vec{\gamma}p \to \pi^+ n$. The pion center-of-mass production angle is shown. Notation as in Fig. 10.

also indicates that the fit to the previously published Σ data is actually improved slightly in DU13 versus CM12, decreasing to 3.67 from 3.99. This is due to the added weighting of the Σ data reported here in the fit, and also provides additional statistical confirmation of the consistency of the overall present and prior measurements, despite the differences noted above.

In Figs. 15–20 (shown in Appendix B), we compare the dominant multipole contributions from SAID (CM12 and DU13), MAID, and BnGa. While the CM12 and DU13 solutions differ over the energy range of this experiment, the resonance couplings are fairly stable. The largest change is found for the $\Delta(1700)3/2^-$ and $\Delta(1905)5/2^+$ states (Table III), for which the various analyses disagree significantly in terms of photo-decay amplitudes.

The reason that MAID better describes the neutral-pion data but misses the charged-pion data appears to be tied partly to the $E_{0+}^{1/2}$ and $E_{0+}^{3/2}$ multipoles. As can be seen in Figs. 15–20, both MAID multipoles differ significantly from the SAID values. In Fig. 13, we plot for comparison the moduli of those linear combinations of isospin amplitudes producing the $E_{0+}^{\pi^0 p}$ and $E_{0+}^{\pi^+ n}$ amplitudes.

B. Associated Legendre function expansion

The photoproduction of a pseudoscalar meson is described by four independent helicity amplitudes, which may be

TABLE III. $\Delta(1700)3/2^-$ and $\Delta(1905)5/2^+$ state Breit-Wigner parameters from SAID (DU13 and CM12 [27]), MAID [28], BnGa [29], and PDG12 [1].

Δ^*	Solution	$A_{1/2}$ ($\text{GeV}^{1/2} \times 10^{-3}$)	$A_{3/2}$ ($\text{GeV}^{1/2} \times 10^{-3}$)
$\Delta(1700)3/2^-$	CM12	105 ± 5	92 ± 4
	DU13	132 ± 5	108 ± 5
	BnGa	160 ± 20	165 ± 25
	MD07	226	210
	PDG12	104 ± 15	85 ± 22
$\Delta(1905)5/2^+$	CM12	19 ± 2	-38 ± 4
	DU13	20 ± 2	-49 ± 5
	BnGa	25 ± 5	-49 ± 4
	MD07	18	-28
	PDG12	26 ± 11	-45 ± 20

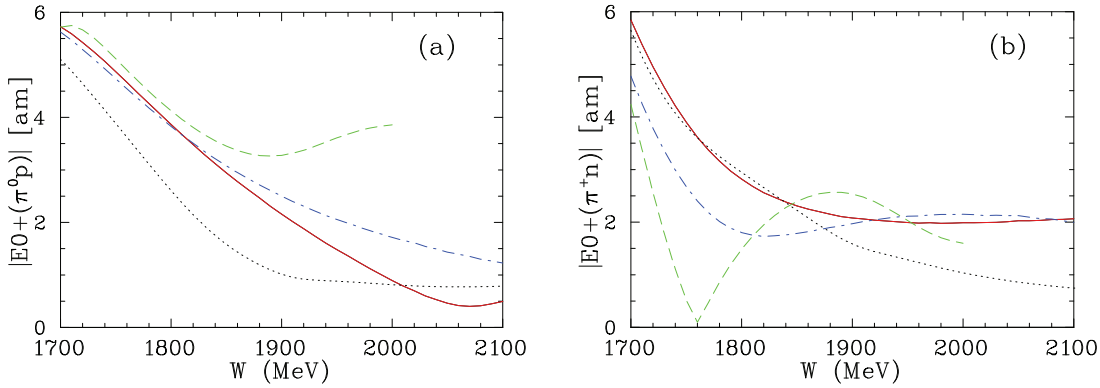

FIG. 13. (Color online) Moduli of the (a) $E_{0+}(\pi^0 p)$ and (b) $E_{0+}(\pi^+ n)$ amplitudes. Notation is the same as in Fig. 15.

decomposed over Wigner harmonics $d^j_{\lambda\mu}(\theta)$ [32]. After Barker *et al.* [33,34], those amplitudes are commonly denoted N, S_1, S_2, and D, where $\mu = 1/2$ and $\lambda = +1/2, -1/2, +3/2, -3/2$, respectively. The amplitude N is the nonflip helicity amplitude, the S amplitudes correspond to the single-flip helicity amplitudes, and the D amplitude corresponds to the double-flip helicity amplitude. The beam asymmetry Σ is related to these helicity amplitudes by the relation [34]

$$[\Sigma d\sigma/d\Omega] \sim 2\mathrm{Re}[S_1^* S_2 - N D^*]. \tag{3}$$

The first summand of this relation contains terms with products $d^{j_1}_{3/2,1/2} d^{j_2}_{-1/2,1/2}$, while the second contains products $d^{j_1}_{1/2,1/2} d^{j_2}_{-3/2,1/2}$. These products yield Clebsch-Gordan series over the associated second-order Legendre functions $P^2_j(\theta)$, with the degree j given by $|j_1 - j_2| \leqslant j \leqslant j_1 + j_2$ [32]. The beam asymmetry as a whole, then, may be represented by an infinite series over these second-order associated Legendre functions of degree j, with the degree j running from $j = 2$ to infinity, after recalling that j should not be less than 2.

We have used such a series to fit the data on the beam asymmetry Σ reported here, supplemented by the fact that $\Sigma(0) = \Sigma(\pi) = 0$. The small statistical uncertainties of the data obtained here allow a correspondingly robust determination of the second-order associated Legendre function coefficients A_j; these coefficients were very difficult to determine unambiguously with previously published data of lower statistical accuracy. The results of our fits yield unprecedented detail on the energy dependence of the Legendre coefficients A_j, and should prove very useful in disentangling the helicity amplitudes associated with pion photoproduction for the present energy range.

As expected for such a fit using orthogonal polynomials, the Legendre coefficients A_j decrease markedly for large j. At our energies and precision, a maximum value of $j = 10$ was

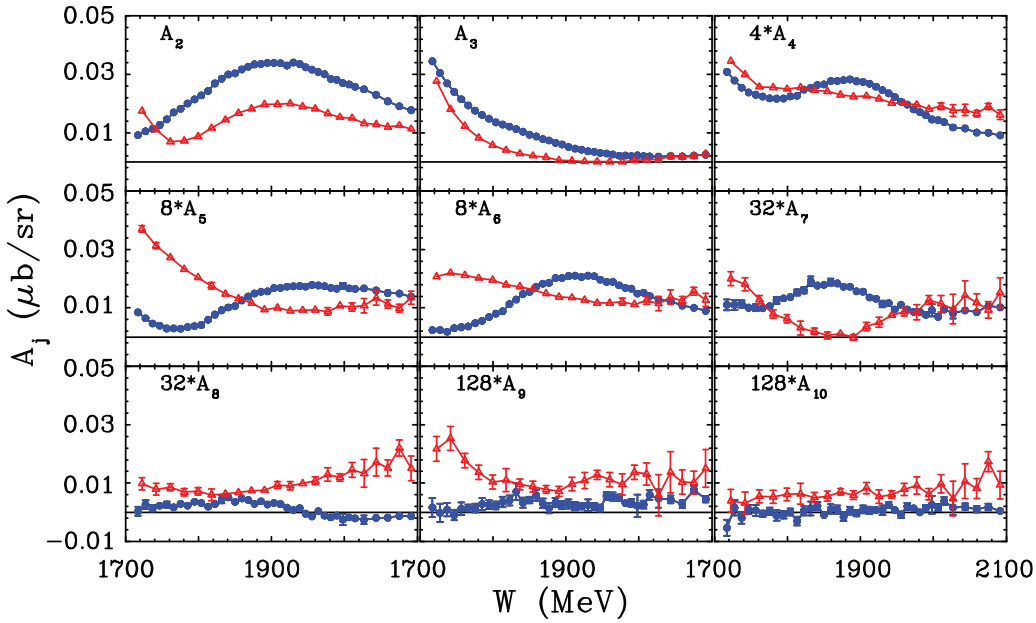

FIG. 14. (Color online) Coefficients for associated Legendre functions of the second order for $\pi^0 p$ (solid circles) and $\pi^+ n$ (solid triangles). Solid lines are plotted to help guide the eye.

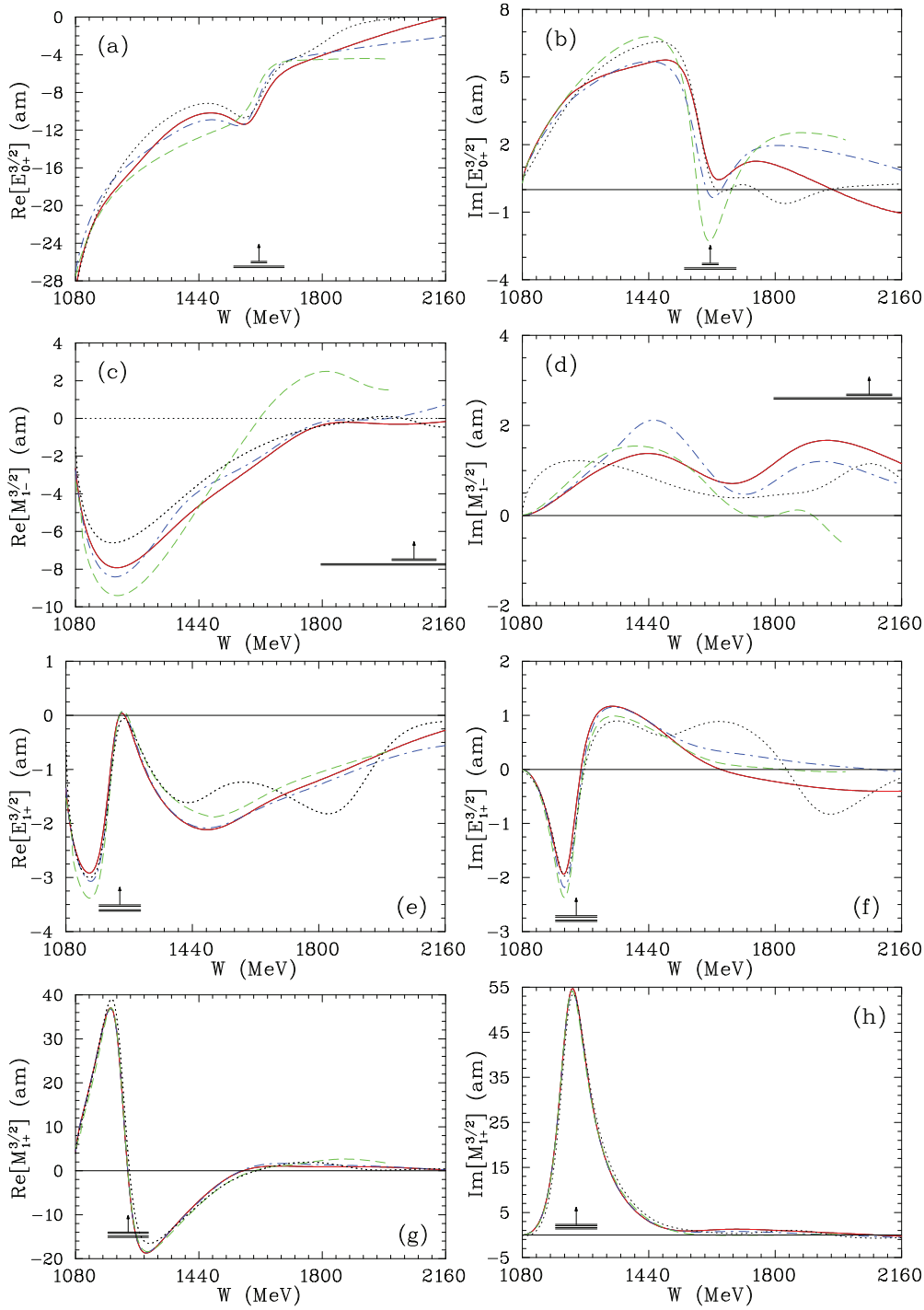

FIG. 15. (Color online) Isospin $I = 3/2$ multipole amplitudes from threshold to $W = 2.16$ GeV ($E_\gamma = 2.02$ GeV) for $l = 0,1$. Solid (dash-dotted) lines correspond to the SAID DU13 (CM12 [27]) solution. Dashed (short-dashed) lines give MAID07 [28], which terminates at $W = 2$ GeV (BG2011-02 BnGa solution [29]). Vertical arrows indicate resonance energies W_R and horizontal bars show full (Γ) and partial ($\Gamma_{\pi N}$) widths associated with the SAID πN solution SP06 [31].

found to be sufficient to describe the data. Thus, we truncate the infinite series accordingly, using the relation

$$[\Sigma d\sigma/d\Omega](\cos\theta) = \sum_{j=2}^{10}(2j+1)A_j P_j^2(\cos\theta),$$

where the degree j runs from 2–10.

In Fig. 14, we illustrate Legendre coefficients A_2–A_{10} as a function of center-of-mass energy W from the best fit of the product of the experimental CLAS Σ data provided by this work and DU13 predictions for $d\sigma/d\Omega$. None of the coefficients show a narrow structure in the energy dependence. However, wide structures are clearly seen in the range $W = 1.8$–2.0 GeV, most likely attributable to contributions

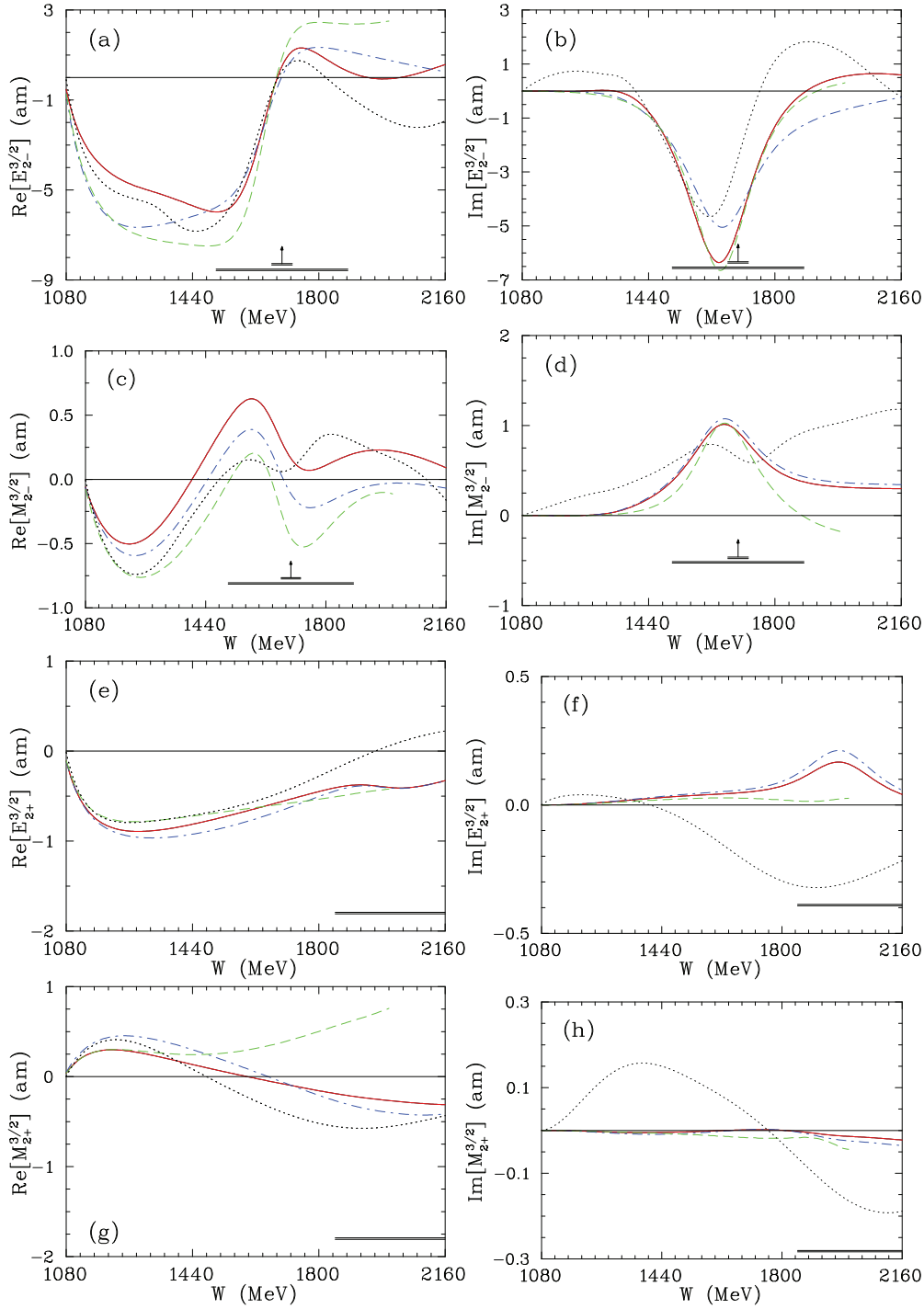

FIG. 16. (Color online) Isospin $I = 3/2$ multipole amplitudes from threshold to $W = 2.16$ GeV ($E_\gamma = 2.02$ GeV) for $l = 2$. Notation as in Fig. 15.

from one or more nucleon resonances known in this energy region with spins up to 7/2. [1] It is interesting that the coefficients A_3 for both final states have no energy structures at all; they are smooth functions throughout this energy region, with no evidence of the structures seen for the other coefficients.

For the $\pi^+ n$ final state, the behavior of the A_j is noticeably different for most of the coefficients than the behavior observed for the $\pi^0 p$ final state. The energy dependence of the A_2 term for the $\pi^+ n$ final state has a similar, though smaller, bump as seen in the neutral pion data. Likewise, the A_3 coefficients for both the $\pi^+ n$ and $\pi^0 p$ final states show similar energy behavior. The energy dependences of the A_4–A_8 coefficients for the $\pi^+ n$ final state are seen to lack the narrow structures seen for the $\pi^0 p$ final state. Moreover, the A_8 coefficient for the neutral pion changes sign near $W = 1950$ MeV, while staying positive for the $\pi^+ n$ case.

These pronounced differences between charged and neutral pion reactions reveal the essential role of the interferences

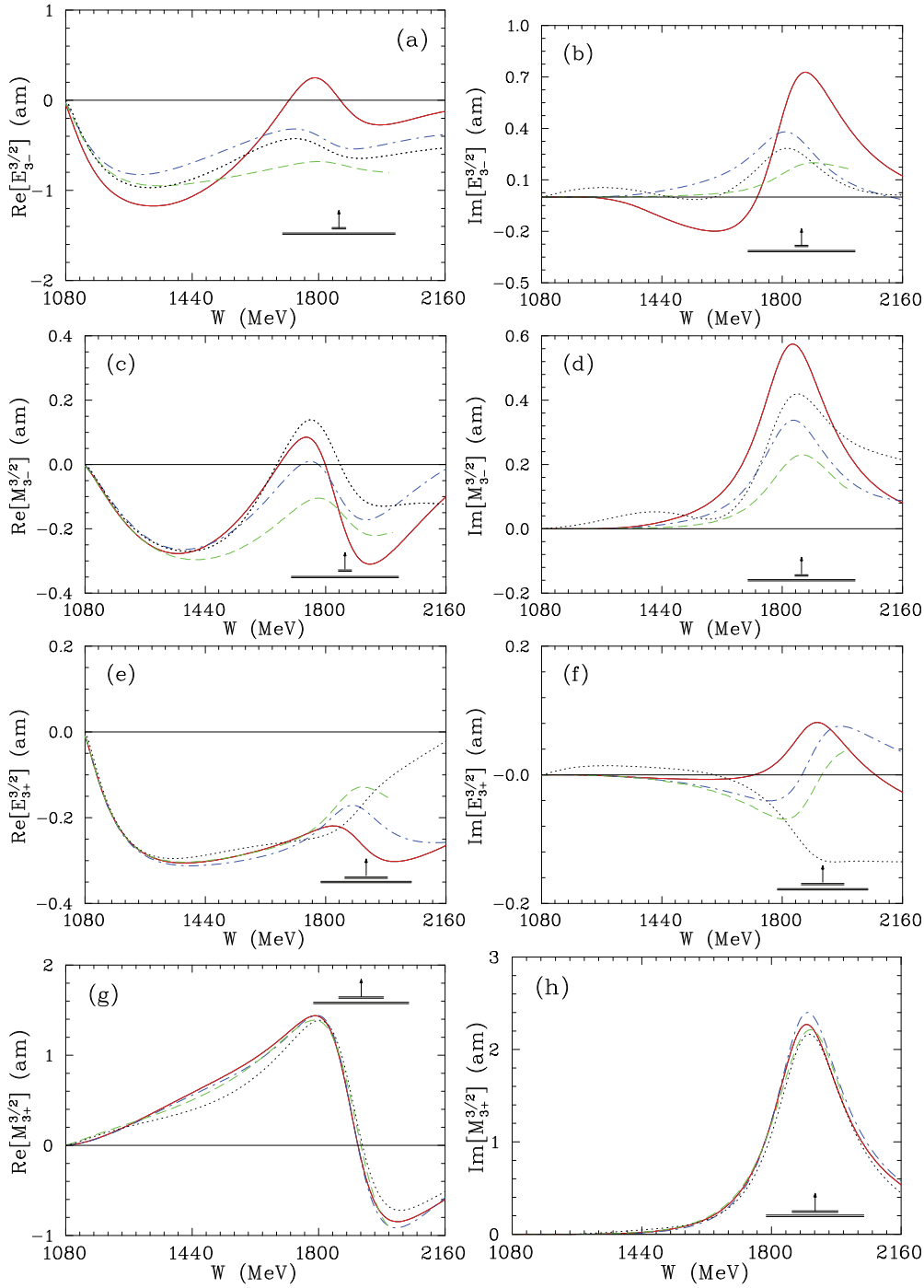

FIG. 17. (Color online) Isospin $I = 3/2$ multipole amplitudes from threshold to $W = 2.16$ GeV ($E_\gamma = 2.02$ GeV) for $l = 3$. Notation as in Fig. 15.

between the photoproduction amplitudes for the two final states with isospin $1/2$ and $3/2$. Energy structures are less clear for the coefficients A_9 and A_{10}. The A_{10} coefficients, especially for the neutral pion, are statistically consistent with zero, thus justifying our truncation of the Legendre series.

The pion production angles 60° and 120° are mirror angles, which reveal dynamics associated with the interference of several amplitudes having different angular momenta. The sharpness of both dips seen in the Σ data indicates that important contributions must come from partial waves with large j.

This analysis of the angular dependence of the beam asymmetry data in terms of associated Legendre functions reinforces the long-recognized complexity of the nucleon resonance spectrum in this energy region. That complexity underscores the point that an accurate interpretation of beam asymmetry in pion photoproduction will require a comprehensive account of the amplitude interference effects both in

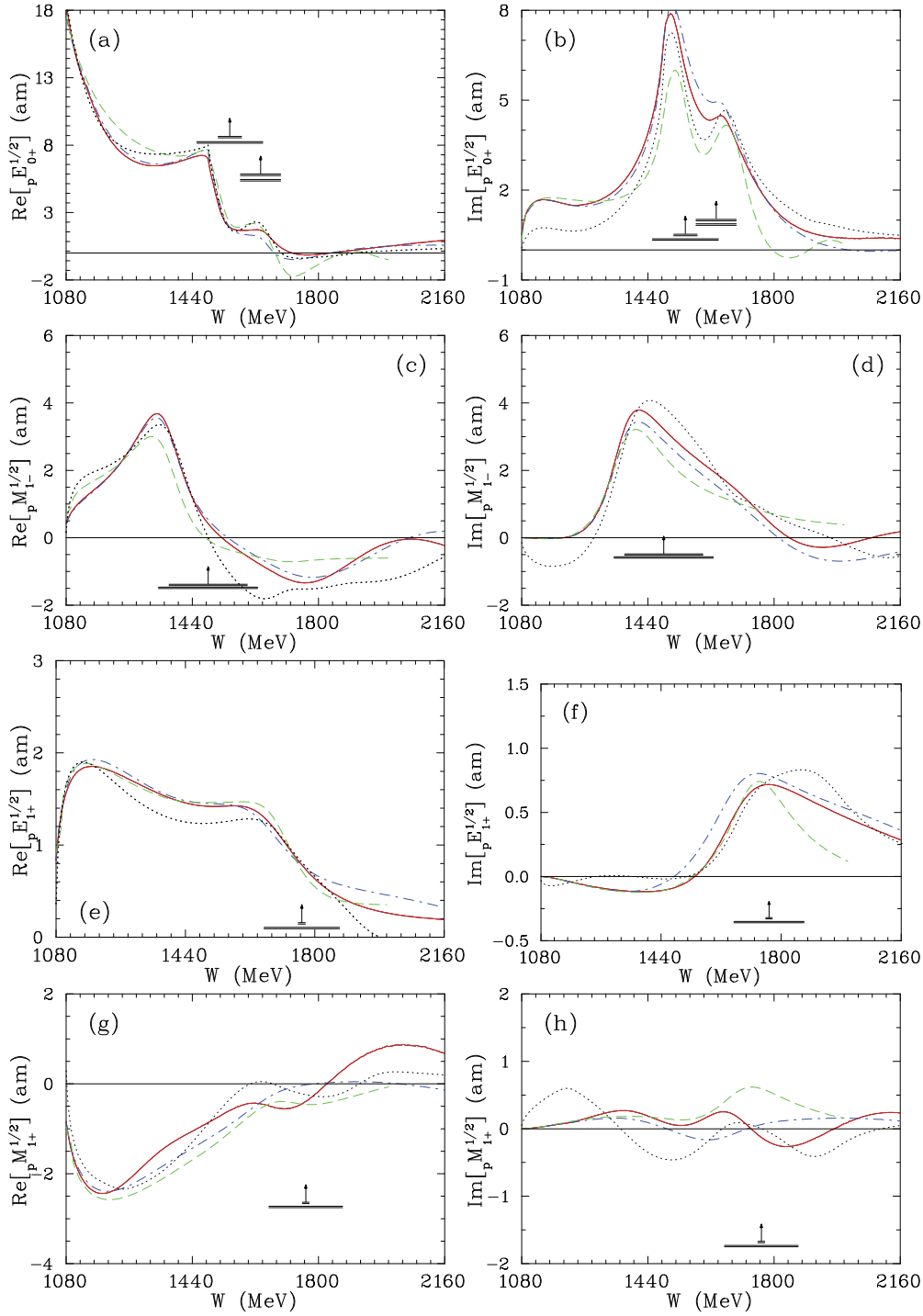

FIG. 18. (Color online) Proton multipole $I = 1/2$ amplitudes from threshold to $W = 2.16$ GeV ($E_\gamma = 2.02$ GeV) for $l = 0,1$. Notation as in Fig. 15.

terms of angular momentum j and isospin. The complicated interplay of the contributions from the different resonances demands further clarification through measurements of other polarization observables in order to isolate contributions to particular amplitudes. For example, the expression in Eq. (3) above for the beam asymmetry Σ in terms of N, S_1, S_2, and D from Ref. [34] may be compared to the expression from the same reference for the double-polarized observable G,

$$[Gd\sigma/d\Omega] \sim 2\mathrm{Im}[S_1^* S_2 - N D^*].$$

Thus, the combination of Σ and G data greatly facilitates isolating the individual contributions of each helicity amplitude. New data on polarization observables have been taken [35] in Hall B at Jefferson Laboratory using a polarized target (transverse and longitudinal) with polarized photon beams

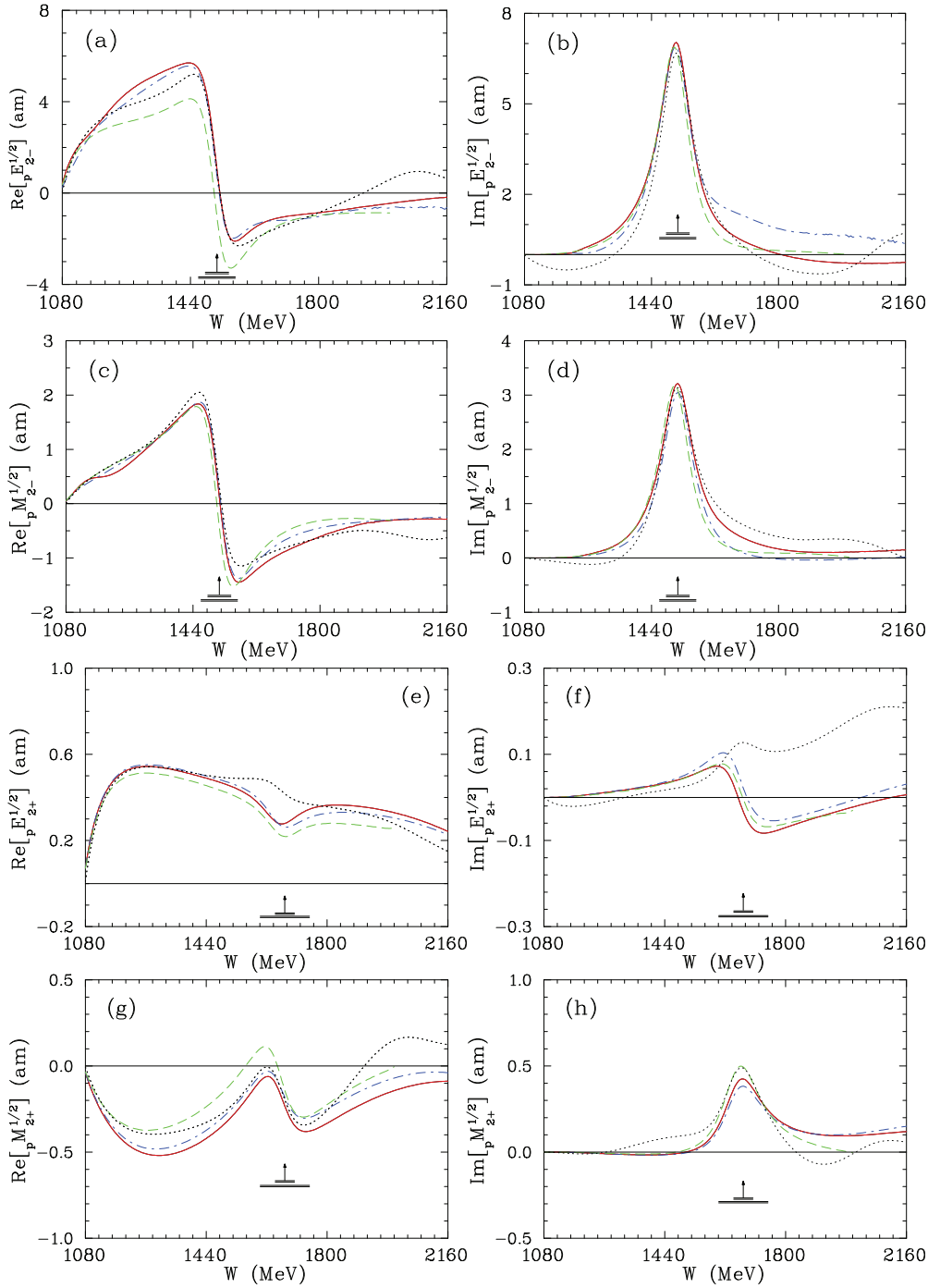

FIG. 19. (Color online) Proton multipole $I = 1/2$ amplitudes from threshold to $W = 2.16$ GeV ($E_\gamma = 2.02$ GeV) for $l = 2$. Notation as in Fig. 15.

(circular and linear) that are currently undergoing analysis for the observables G, F, T, P. The information from these observables, coupled with the detailed results obtained here for Σ, will permit tremendous progress in deconvoluting the nucleon resonance spectrum.

XI. CONCLUSION

Knowing the precise details of the proton's excitation spectrum is essential for establishing a comprehensive understanding of the QCD structure of the nucleon. Our knowledge of nucleon excitations is quite incomplete, with some states felt to be well established, and many others known with less (or even much less) confidence. A significant increase in the comprehensiveness of the database for observables in the meson photoproduction process is critical to reaching definitive knowledge about the resonance spectrum and, in turn, improving any QCD-based model of the nucleon. Studies that cover a broad range of center-of-mass energy W are

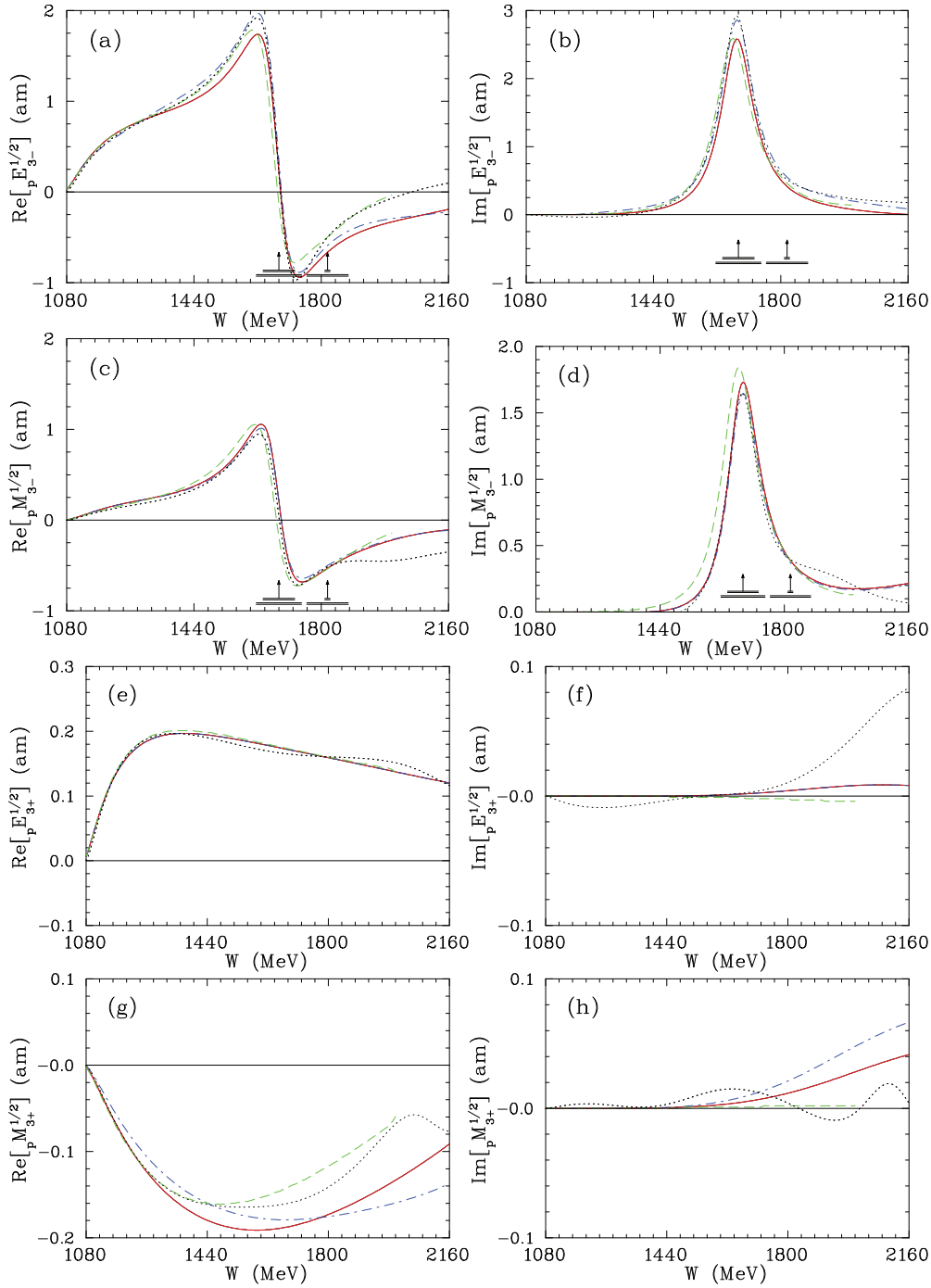

FIG. 20. (Color online) Proton multipole $I = 1/2$ amplitudes from threshold to $W = 2.16$ GeV ($E_\gamma = 2.02$ GeV) for $l = 3$. Notation as in Fig. 15.

particularly helpful in sorting out the broad and overlapping spectrum of states.

Through the experiments described above, an extensive and precise data set (1086 data points) on the beam asymmetry Σ for π^0 and π^+ photoproduction from the proton has been obtained over the range of $1.10\,\text{GeV} \leqslant W \leqslant 1.86\,\text{GeV}$. A novel approach based on the use of Fourier moments was employed for extracting the beam asymmetries from the experimental data, and the technique is described in an accompanying appendix.

The measurements obtained here have been compared to existing data. The overall agreement is good, while the data provided here more than double the world database for both pion reactions, are more precise than previous measurements, and cover the reported energies with finer resolution.

By comparing this new and greatly expanded data set to the predictions of several semiempirical models for the nucleon resonance spectrum, the present data were found to favor the SAID and Bonn-Gatchina analyses over the older MAID predictions for both reactions. The present set of beam

asymmetries has been incorporated into the SAID database, and exploratory fits have been made, resulting in a significant improvement in the fit χ-squared, and allowing for a much improved mapping of the sharp structure near 60° and less sharp one near 120° at photon energies greater than about 1600 MeV. Resonance couplings have been extracted and the largest change from previous fits was found to occur for the $\Delta(1700)3/2^-$ and $\Delta(1905)5/2^+$ states. Surprisingly, these two resonances, respectively, are considered "three-star" and "four-star" states in the Particle Data Group summary table [1]. That the largest changes were found for these well-established and, by inference, well-known excitations underscores the provisional nature of our current understanding of the nucleon resonance spectrum, and urgently motivates further experimental studies on all accessible observables for the meson photoproduction process.

Beyond these phenomenological analyses, we performed an analysis of our beam asymmetry data using a series based on associated Legendre functions, coupled with predictions for the differential cross sections provided by SAID. This fit was made possible by the high statistical accuracy and broad W coverage of the current data set. The analysis clearly shows the important role of interference contributions coming from the isospin 1/2 and 3/2 basis states to the π^0 and π^+ photoproduction reactions. When combined with future measurements of G, these data should greatly further attempts to disentangle the contributions of various resonances to the photoproduction process, and thereby promote significant progress in elucidating the QCD structure of the nucleon.

ACKNOWLEDGMENTS

The authors gratefully acknowledge the work of the Jefferson Lab Accelerator Division staff. This work was supported by the National Science Foundation, the U.S. Department of Energy (DOE), the French Centre National de la Recherche Scientifique and Commissariat à l'Energie Atomique, the Italian Istituto Nazionale di Fisica Nucleare, the United Kingdom's Science and Technology Facilities Council (STFC), and the National Research Foundation of Korea. The Southeastern Universities Research Association (SURA) operated Jefferson Lab for DOE under Contract No. DE-AC05-84ER40150 during this work.

APPENDIX A: FOURIER MOMENT TECHNIQUE FOR EXTRACTING BEAM ASYMMETRY Σ

1. Definition of observables

Meson photoproduction differential cross sections may be written as

$$\frac{d^2\sigma}{d\Omega dE_\gamma},$$

where dE_γ is the infinitesimal incident photon energy bin width and $d\Omega$ is the infinitesimal solid angle element in which the photoproduced meson is detected. (All quantities are center-of-mass quantities unless otherwise indicated.) Practically, however, the cross sections are measured in terms of finite kinematic bins in photon energy and scattering angle. Thus, what is measured is more accurately written

$$\Delta\sigma^{i,j,k} = \int_{E_{i-1}}^{E_i}\int_{\theta_{j-1}}^{\theta_j}\int_{\varphi_{k-1}}^{\varphi_k} \frac{d^2\sigma}{d\cos(\theta)dE_\gamma} dE_\gamma \sin(\theta) d\theta d\varphi, \tag{A1}$$

where the indices i, j, and k denote the individual bin boundaries for incident photon energy E_γ, scattering polar angle θ, and azimuthal scattering angle φ, respectively.

Experimentally, $\Delta\sigma^{i,j,k}$ in Eq. (A1) is approximated by the relation

$$\Delta\sigma^{i,j,k} \approx \frac{Y^{i,j,k}}{N_\gamma^i \rho L \epsilon^{i,j,k}}, \tag{A2}$$

where $Y^{i,j,k}$ is the meson yield in kinematic bin i,j,k, N_γ^i is the incident number of photons for bin i, ρ is the target density, L is the target length, and $\epsilon^{i,j,k}$ is the detector efficiency for kinematic bin i,j,k.

As defined above, the photon beam polarization orientations used for the running period had either the electric field vector parallel to the Hall B floor (with the degree of polarization denoted by $P_\parallel$) or perpendicular to the floor (with the corresponding degree of polarization $P_\perp$). The differential cross sections for the various incident photon beam polarizations are labeled in the following fashion:

(a) for perpendicular beam polarization,

$$\frac{d\sigma_\perp}{d\Omega} = \frac{d\sigma_a}{d\Omega}[1 + P_\perp \Sigma \cos(2\varphi)]; \tag{A3}$$

(b) for parallel beam polarization,

$$\frac{d\sigma_\parallel}{d\Omega} = \frac{d\sigma_a}{d\Omega}[1 - P_\parallel \Sigma \cos(2\varphi)]. \tag{A4}$$

The unpolarized differential cross sections for a given reaction extracted from the amorphous carbon radiator is

$$\frac{d\sigma_a}{d\Omega} = \frac{1}{2}\left(\frac{d\sigma_\perp}{d\Omega} + \frac{d\sigma_\parallel}{d\Omega}\right). \tag{A5}$$

2. Azimuthal moments for determining Σ

For this analysis, two additional φ-dependent quantities are defined:

$$f^{i,j}(\varphi) = \rho L \int_{E_{i-1}}^{E_i}\int_{\theta_{j-1}}^{\theta_j} \epsilon(E_\gamma,\theta,\varphi)\frac{d^2\sigma}{d\Omega dE_\gamma} dE_\gamma \sin\theta d\theta$$

and

$$\tilde{Y}^{i,j}(\varphi) = \frac{Y^{i,j}(\varphi)}{N_\gamma^i}, \tag{A6}$$

where the former defines the normalized yield density with respect to azimuthal angle, and the latter is simply the normalized yield for a given φ for bin i,j. These normalized yields may be further labeled by the photon beam polarization as $\tilde{Y}_a^{i,j}$, $\tilde{Y}_\perp^{i,j}$, and $\tilde{Y}_\parallel^{i,j}$, which would be the yield for the amorphous target, the yield with the perpendicularly polarized beam, and the yield with the parallel polarized beam, respectively.

Using the appropriate definitions given in Eqs. (A3), (A4), and (A5), the three normalized yields in Eqs. (A6) may be written as

$$\tilde{Y}_a^{i,j} = \int_0^{2\pi} f_a^{i,j}(\varphi)d\varphi, \tag{A7}$$

$$\tilde{Y}_\perp^{i,j} = \int_0^{2\pi} f_a^{i,j}(\varphi)[1 + P_\perp^i \Sigma^{i,j}\cos(2\varphi)]d\varphi, \tag{A8}$$

$$\tilde{Y}_\parallel^{i,j} = \int_0^{2\pi} f_a^{i,j}(\varphi)[1 - P_\parallel^i \Sigma^{i,j}\cos(2\varphi)]d\varphi. \tag{A9}$$

With these definitions, *all* yields are now expressed in terms of various integrals involving the normalized yield density $f_a^{i,j}(\varphi)$, which is the normalized yield density for the *amorphous* carbon radiator. This function includes all physics effects modulated by the experimental acceptance $\epsilon^{i,j}$. The quantity $f_a^{i,j}(\varphi)$ is then expanded in a Fourier series as

$$f_a^{i,j}(\varphi) = a_0 + \sum_{n=1}^{\infty}[a_n\cos(n\varphi) + b_n\sin(n\varphi)], \tag{A10}$$

where each term of the series represents the nth Fourier moment of $f_a^{i,j}$.

As usual, one can construct, event by event, a missing mass histogram for the reaction $\gamma p \to pX$ or $\gamma p \to \pi^+ X$. In the approach used here, moment-n histograms are constructed by taking each event in the $\gamma p \to pX$ or $\gamma p \to \pi^+ X$ missing mass histogram and weighting each event by the value of $\cos(n\varphi)$ corresponding to that event for the various yields in (A7)–(A9).

Of particular importance are the moment-2 histograms

$$\begin{aligned}\tilde{Y}_{\perp 2}^{i,j} &\equiv \int_0^{2\pi} f_\perp^{i,j}(\varphi)\cos(2\varphi)d\varphi \\ &= \int_0^{2\pi} f_a^{i,j}(\varphi)\cos(2\varphi)d\varphi \\ &\quad + P_\perp \Sigma^{i,j}\int_0^{2\pi} f_a^{i,j}(\varphi)\cos^2(2\varphi)d\varphi\end{aligned} \tag{A11}$$

and

$$\begin{aligned}\tilde{Y}_{\parallel 2}^{i,j} &\equiv \int_0^{2\pi} f_\parallel^{i,j}(\varphi)\cos(2\varphi)d\varphi \\ &= \int_0^{2\pi} f_a^{i,j}(\varphi)\cos(2\varphi)d\varphi \\ &\quad - P_\parallel \Sigma^{i,j}\int_0^{2\pi} f_a^{i,j}(\varphi)\cos^2(2\varphi)d\varphi.\end{aligned} \tag{A12}$$

Subtracting Eq. (A12) from (A11) yields

$$\begin{aligned}\tilde{Y}_\Sigma^{i,j} &\equiv \tilde{Y}_{\perp 2}^{i,j} - \tilde{Y}_{\parallel 2}^{i,j} \\ &= (P_\perp^i + P_\parallel^i)\Sigma^{i,j}\int_0^{2\pi} f_a^{i,j}(\varphi)\cos^2(2\varphi)d\varphi.\end{aligned} \tag{A13}$$

Using the double-angle relationship for the cosine of an angle, and keeping the Fourier series definition of $f_a^{i,j}(\varphi)$ from Eq. (A10) in mind, this can be rewritten as

$$\tilde{Y}_\Sigma^{i,j} = \pi(P_\perp^i + P_\parallel^i)\Sigma^{i,j}\left(a_0 + \frac{a_4}{2}\right). \tag{A14}$$

The polarization varies continuously during the course of a typical data run owing to fluctuations in the relative alignment of the incident electron beam and the diamond. Thus, the polarization must be determined continuously during a data run so that a photon-flux-weighted equivalent value of polarization for each run can be determined. The values of $P_\parallel$ and $P_\perp$ used in these equations are assumed to be these photon-flux-weighted values.

With these photon-flux-weighted equivalent values for the polarization $P_\parallel$ and $P_\perp$ and the histogram defined by Eq. (A14), one only needs the Fourier coefficients a_0 and a_4 for $f_a^{i,j}(\varphi)$ to determine $\tilde{Y}_\Sigma^{i,j}$.

Obtaining the quantity $(a_0 + \frac{a_4}{2})$ in Eq. (A14) is straightforward using other moment-n histograms. In a manner similar to that leading to Eqs. (A11) and (A12), one obtains for the moment-0 histograms

$$\tilde{Y}_{\perp 0}^{i,j} = 2\pi a_0 + P_\perp^i \Sigma^{i,j}\pi a_2$$

and

$$\tilde{Y}_{\parallel 0}^{i,j} = 2\pi a_0 - P_\parallel^i \Sigma^{i,j}\pi a_2,$$

which gives

$$\tilde{Y}_{\perp 0}^{i,j} + \tilde{Y}_{\parallel 0}^{i,j}\left(\frac{P_\perp^i}{P_\parallel^i}\right) = 2\pi a_0\left(1 + \frac{P_\perp^i}{P_\parallel^i}\right). \tag{A15}$$

In a similar fashion, one obtains from the moment-4 histograms

$$\tilde{Y}_{\perp 4}^{i,j} + \tilde{Y}_{\parallel 4}^{i,j}\left(\frac{P_\perp^i}{P_\parallel^i}\right) = \pi a_4\left(1 + \frac{P_\perp^i}{P_\parallel^i}\right). \tag{A16}$$

Finally, using the results of Eqs. (A14)–(A16), one obtains

$$\tilde{Y}_\Sigma^{i,j} = \Sigma^{i,j}\left\{\frac{P_\parallel^i}{2}\left(\tilde{Y}_{\perp 0}^{i,j} + \tilde{Y}_{\perp 4}^{i,j}\right) + \frac{P_\perp^i}{2}\left(\tilde{Y}_{\parallel 0}^{i,j} + \tilde{Y}_{\parallel 4}^{i,j}\right)\right\}. \tag{A17}$$

Combining Eqs. (A13) and (A17), the beam asymmetry Σ for kinematic bin i, j is found to be

$$\Sigma^{i,j} = \frac{\tilde{Y}_{\perp 2}^{i,j} - \tilde{Y}_{\parallel 2}^{i,j}}{\frac{P_\parallel^i}{2}\left(\tilde{Y}_{\perp 0}^{i,j} + \tilde{Y}_{\perp 4}^{i,j}\right) + \frac{P_\perp^i}{2}\left(\tilde{Y}_{\parallel 0}^{i,j} + \tilde{Y}_{\parallel 4}^{i,j}\right)}. \tag{A18}$$

However, as it stands, the value of $\Sigma^{i,j}$ generated by the ratio in Eq. (A18) is the beam asymmetry for whatever is in that particular kinematic bin, which will include not only the particular peak of interest but also any background within that particular kinematic bin. The interest here, instead, is the beam asymmetry associated with the photoproduction of a particular meson, which appears as a peak in the missing mass spectrum, and not the associated background beneath that peak. In practice, then, one extracts from the various histograms in the numerator and denominator in Eq. (A18) the yield of the particular meson peak corresponding to the reaction of interest.

In order to simplify the notation below, the incident photon energy bin index i and $\cos(\theta)$ bin index j will be suppressed hereafter. The beam asymmetry is thus written as

$$\Sigma = \frac{\tilde{Y}_{\perp 2} - \tilde{Y}_{\parallel 2}}{\frac{P_\parallel}{2}(\tilde{Y}_{\perp 0} + \tilde{Y}_{\perp 4}) + \frac{P_\perp}{2}(\tilde{Y}_{\parallel 0} + \tilde{Y}_{\parallel 4})}. \tag{A19}$$

Equation (A19) is the principal result for this method. With this approach, rather than partitioning the data for a given E_γ and $\cos(\theta)$ into various φ bins, all the data for a given E_γ and $\cos(\theta)$ are used simultaneously to determine the beam asymmetry Σ for the reaction of interest.

3. Statistical uncertainty

Because the various components of Eq. (A19) have nonvanishing covariances, the determination of statistical uncertainties, while straightforward, requires attention.

We begin by defining $w_{m,k,l}$ as the histogram weighting of the lth Poisson-distributed event, of the mth moment within the kth mass bin of a moment histogram $\tilde{Y}_m$. It then follows that the total occupancy $\tilde{Y}_{m,k}$ of the kth bin within $\tilde{Y}_m$ is

$$\tilde{Y}_{m,k} = \frac{1}{N_\gamma}\sum_{l=1}^{Y_{0,k}} w_{m,k,l},$$

where $Y_{0,k}$ is the total number of events in bin k. For $m = 0$ this is simply

$$\tilde{Y}_{0,k} = \frac{1}{N_\gamma}\sum_{l=1}^{Y_{0,k}} 1 = \frac{Y_{0,k}}{N_\gamma},$$

as expected. For all other moments

$$\tilde{Y}_{m,k} = \frac{1}{N_\gamma}\sum_{l=1}^{Y_{0,k}} \cos(m\varphi_l).$$

It now follows that the variance $\sigma^2_{\tilde{Y}_{m,k}}$ is given by

$$\sigma^2_{\tilde{Y}_{m,k}} = \frac{1}{(N_\gamma)^2}\sum_{l=1}^{Y_{0,k}} \cos^2(m\varphi_l),$$

which for $m = 0$, reduces to the familiar form for a Poisson-distributed random variable divided by a constant term N_γ,

$$\sigma^2_{\tilde{Y}_{0,k}} = \frac{1}{(N_\gamma)^2}\sum_{l=1}^{Y_{0,k}} 1 = \frac{1}{(N_\gamma)^2} Y_{0,k} = \frac{1}{N_\gamma}\tilde{Y}_{0,k}.$$

It is useful to note that, by way of the double-angle relationship for the cosine of an angle, the variance of $\tilde{Y}_{m,k}$ can be written as

$$\sigma^2_{\tilde{Y}_{m,k}} = \frac{1}{2(N_\gamma)^2}\sum_{l=1}^{Y_{0,k}} [1 + \cos(2m\varphi_l)] = \frac{1}{2N_\gamma}[\tilde{Y}_{0,k} + \tilde{Y}_{2m,k}].$$

The covariance of two variables $\tilde{Y}_{m1,k}$, and $\tilde{Y}_{m2,k}$, $\mathrm{Cov}(\tilde{Y}_{m_1,k}, \tilde{Y}_{m_2,k})$, is given by

$$\mathrm{Cov}\left(\tilde{Y}_{m_1,k}, \tilde{Y}_{m_2,k}\right) = \frac{1}{(N_\gamma)^2}\sum_{l=1}^{Y_{0,k}} \cos(m_1\varphi_l)\cos(m_2\varphi_l).$$

In what follows the identity

$$\begin{aligned}\mathrm{Cov}(\tilde{Y}_{m,k}, \tilde{Y}_{2m,k}) &= \frac{1}{(N_\gamma)^2}\sum_{l=1}^{Y_{0,k}} \cos(m\varphi_l)\cos(2m\varphi_l) \\ &= \frac{1}{(N_\gamma)^2}\sum_{l=1}^{Y_{0,k}} \frac{1}{2}(\cos(m\varphi_l) + \cos(3m\varphi_l)) \\ &= \frac{1}{2(N_\gamma)^2}(\tilde{Y}_{m,k} + \tilde{Y}_{3m,k})\end{aligned}$$

will be of use, as well as

$$\mathrm{Cov}(\tilde{Y}_{0,k}, \tilde{Y}_{m,k}) = \frac{1}{N_\gamma}\tilde{Y}_{m,k}.$$

With these preliminaries, the statistical uncertainty for the beam asymmetry Σ given by Eq. (A19) can be determined.

By allowing the following definitions of the numerator and denominator of Eq. (A19),

$$\begin{aligned} n &\equiv \tilde{Y}_{\perp 2} - \tilde{Y}_{\parallel 2} \\ d &\equiv \frac{P^i_\parallel}{2}(\tilde{Y}_{\perp 0} + \tilde{Y}_{\perp 4}) + \frac{P^i_\perp}{2}(\tilde{Y}_{\parallel 0} + \tilde{Y}_{\parallel 4}),\end{aligned} \tag{A20}$$

we can then rewrite the beam asymmetry Σ in the form

$$\Sigma = \frac{n}{d}.$$

The variance of Σ is then

$$\sigma^2_\Sigma = \Sigma^2\left\{\frac{\sigma^2_n}{n^2} + \frac{\sigma^2_d}{d^2} - \frac{2\mathrm{Cov}(n,d)}{nd}\right\}.$$

We can now determine the variance of n, d, and the covariance of n, d. The variance of n is

$$\sigma^2_n = \frac{1}{2N_{\gamma\perp}}(\tilde{Y}_{\perp 0} + \tilde{Y}_{\perp 4}) + \frac{1}{2N_{\gamma\parallel}}(\tilde{Y}_{\parallel 0} + \tilde{Y}_{\parallel 4}),$$

where $N_{\gamma\perp}$ ($N_{\gamma\parallel}$) is the integrated photon flux for perpendicular (parallel) photon beam orientation. The variance of d is

$$\begin{aligned}\sigma^2_d = &\frac{P^2_\parallel}{4N_{\gamma\perp}}\left(\tilde{Y}_{\perp 0} + \frac{1}{2}(\tilde{Y}_{\perp 0} + \tilde{Y}_{\perp 8}) + 2\tilde{Y}_{\perp 4}\right) \\ &+ \frac{P^2_\perp}{4N_{\gamma\parallel}}\left(\tilde{Y}_{\parallel 0} + \frac{1}{2}(\tilde{Y}_{\parallel 0} + \tilde{Y}_{\parallel 8}) + 2\tilde{Y}_{\parallel 4}\right)\end{aligned}$$

and the covariance of n, d

$$\mathrm{Cov}(n,d) = \frac{P_\parallel}{4N_{\gamma\perp}}(3\tilde{Y}_{\perp 2} + \tilde{Y}_{\perp 6}) - \frac{P_\perp}{4N_{\gamma\parallel}}(3\tilde{Y}_{\parallel 2} + \tilde{Y}_{\parallel 6}).$$

All the necessary quantities needed to calculate Σ and the associated uncertainty σ_Σ have now been derived.

APPENDIX B: MULTIPOLE AMPLITUDES

The updated SAID partial-wave analysis described in Sec. X permitted the extraction of the dominant isospin $I = 1/2$ and $I = 3/2$ multipole contributions in the photoproduction process for the reactions $\gamma + p \to p + \pi^0$ and $\gamma + p \to n + \pi^+$. The center-of-mass-energy W dependences of

those dominant multipole contributions are shown here in Figs. 15–20. The locations and widths of nucleon resonances suggested by that analysis are indicated in those figures. Finally, the figures also compare the W dependences found in this with the same quantities obtained in the Bonn-Gatchina [29] and MAID [28] analyses.

[1] J. Beringer *et al.* (Particle Data Group), Phys. Rev. D **86**, 010001 (2012).
[2] D. I. Sober *et al.*, Nucl. Inst. Meth. A **440**, 263 (2000).
[3] B. A. Mecking *et al.* (CLAS Collaboration), Nucl. Inst. Meth. A **503**, 513 (2003).
[4] K. Livingston, CLAS note 2011-020, https://misportal.jlab.org/ul/Physics/Hall-B/clas/viewFile.cfm/2011-020.pdf?documentId=656 (unpublished).
[5] S. Taylor *et al.* (CLAS Collaboration), Nucl. Inst. Meth. A **462**, 484 (2001).
[6] M. D. Mestayer *et al.*, Nucl. Inst. Meth. A **449**, 81 (2000).
[7] E. S. Smith *et al.*, Nucl. Inst. Meth. A **432**, 265 (1999).
[8] E. Pasyuk, CLAS note 2007-008, http://www1.jlab.org/ul/Physics/Hall-B/clas/public/2007-008.pdf (unpublished).
[9] E. Pasyuk, CLAS note 2007-016, http://www1.jlab.org/ul/Physics/Hall-B/clas/public/2007-016.pdf (unpublished).
[10] M. Dugger *et al.* (CLAS Collaboration), Phys. Rev. C **76**, 025211 (2007).
[11] M. Dugger, CLAS note 2012-002, https://misportal.jlab.org/ul/Physics/Hall-B/clas/viewFile.cfm/2012-002.pdf?documentId=668 (unpublished).
[12] D. Elsner *et al.* (CBELSA/TAPS Collaboration), Eur. Phys. J. A **39**, 373 (2009); (private communication).
[13] N. Sparks *et al.* (CBELSA/TAPS Collaboration), Phys. Rev. C **81**, 065210 (2010); (private communication).
[14] L. O. Abrahamian *et al.*, Phys. Lett. B **48**, 463 (1974).
[15] R. O. Avakian *et al.*, Yad. Fiz. **26**, 1014 (1977) [Sov. J. Nucl. Phys. **26**, 537 (1977)].
[16] R. O. Avakian *et al.*, Yad. Fiz. **29**, 1212 (1979) [Sov. J. Nucl. Phys. **29**, 625 (1979)].
[17] R. O. Avakian *et al.*, Yad. Fiz. **38**, 1196 (1983) [Sov. J. Nucl. Phys. **38**, 721 (1983)].
[18] K. Sh. Agababian *et al.*, Yad. Fiz. **50**, 1341 (1989) [Sov. J. Nucl. Phys. **50**, 834 (1989)].
[19] R. O. Avakian *et al.* (unpublished).
[20] O. Bartalini *et al.* (GRAAL Collaboration), Eur. Phys. J. A **26**, 399 (2005).
[21] J. Alspector *et al.*, Phys. Rev. Lett. **28**, 1403 (1972).
[22] P. J. Bussey *et al.*, Nucl. Phys. B **104**, 253 (1976).
[23] P. J. Bussey *et al.*, Nucl. Phys. B **154**, 205 (1979).
[24] M. Sumihama *et al.* (LEPS Collaboration), Phys. Lett. B **657**, 32 (2007); (private communication).
[25] O. Bartalini *et al.* (GRAAL Collaboration), Phys. Lett. B **544**, 113 (2002); (private communication).
[26] L. O. Abrahamian *et al.*, Sov. J. Nucl. Phys. **32**, 66 (1980).
[27] R. L. Workman, M. W. Paris, W. J. Briscoe, and I. I. Strakovsky, Phys. Rev. C **86**, 015202 (2012).
[28] The MAID analyses are available through the Mainz website: `http://wwwkph.kph.uni-mainz.de/MAID/` See also D. Drechsel, S. S. Kamalov, and L. Tiator, Eur. Phys. J. A **34**, 69 (2007).
[29] The Bonn-Gatchina analyses are available through the Bonn website: `http://pwa.hiskp.uni-bonn.de/` See also A. V. Anisovich *et al.*, Eur. Phys. J. A **47**, 153 (2011); **48**, 15 (2012).
[30] W. J. Briscoe, I. I. Strakovsky, and R. L. Workman, Institute of Nuclear Studies of The George Washington University Database; http://gwdac.phys.gwu.edu/analysis/pr_analysis.html
[31] R. A. Arndt, W. J. Briscoe, I. I. Strakovsky, and R. L. Workman, Phys. Rev. C **74**, 045205 (2006).
[32] M. Jacob and G. C. Wick, Ann. Phys. (NY) **7**, 404 (1959).
[33] I. S. Barker, A. Donnachie, and J. K. Storrow, Nucl. Phys. B **79**, 431 (1974).
[34] I. S. Barker, A. Donnachie, and J. K. Storrow, Nucl. Phys. B **95**, 347 (1975).
[35] N. Benmouna, W. J. Briscoe, G. V. O'Rially, I. I. Strakovsky, and S. Strauch, JLab Proposal E-03-105, Newport News, VA, USA, 2003 (unpublished).